UC Irvine
UC Irvine Previously Published Works

Title

Functional Contributions of Strong and Weak Cellular Oscillators to Synchrony and Light-shifted Phase Dynamics.

Permalink

Journal

ISSN

Authors

Roberts, Logan
Leise, Tanya L
Welsh, David K
et al.

Publication Date

DOI

Peer reviewed

Functional Contributions of Strong and Weak Cellular Oscillators to Synchrony and Light-Shifted Phase Dynamics

Journal:	*Journal of Biological Rhythms*
Manuscript ID	JBR-15-0148.R3
Manuscript Type:	Original Article
Date Submitted by the Author:	n/a
Complete List of Authors:	Roberts, Logan; UCI, Physiology and Biophysics Leise, Tanya; Amherst College, Mathematics and Statistics Welsh, David; UCSD, Psychiatry and Center for Circadian Biology; Veterans Affairs San Diego Healthcare System Holmes, Todd; UCI, Physiology and Biophysics
Manuscript Keywords:	Circadian, light, neural circuits, bioluminescence, phase dynamics, model simulations
Abstract:	Light is the primary signal that calibrates circadian neural circuits and thus coordinates daily physiological and behavioral rhythms with solar entrainment cues. Drosophila and mammalian circadian circuits consist of diverse populations of cellular oscillators that exhibit a wide range of dynamic light responses, periods, phases, and degrees of synchrony. How heterogeneous circadian circuits can generate robust physiological rhythms while remaining flexible enough to respond to synchronizing stimuli has long remained enigmatic. Cryptochrome is a short wavelength photoreceptor that is endogenously expressed in approximately half of Drosophila circadian neurons. In a previous study, physiological light response was measured using real-time bioluminescence recordings in Drosophila whole brain explants which remain intrinsically light-sensitive. Here we apply analysis of real-time bioluminescence experimental data to show detailed dynamic ensemble representations of whole circadian circuit light entrainment at single neuron resolution. Organotypic whole brain explants were either maintained in constant darkness (DD) for 6 days or exposed to a phase advancing light pulse on the second day. We find that stronger circadian oscillators support robust overall circuit rhythmicity in DD, whereas weaker oscillators can be pushed toward transient desynchrony and damped amplitude to facilitate a new state of phase-shifted network synchrony. Additionally, we employ mathematical modeling to examine how a network composed of distinct oscillator types can give rise to complex dynamic signatures in DD conditions and in response to simulated light pulses. Simulations suggest that complementary coupling mechanisms and a combination of strong and weak oscillators may enable a robust yet flexible circadian network that promotes both synchrony and entrainment. A more complete understanding of how the properties of oscillators and their signaling mechanisms facilitate their distinct roles in light entrainment may allow us to direct and augment the circadian system to speed recovery from jet lag, shift work, and seasonal affective disorder.

1
2
3
4
5
6
7
8
9
10
11
12
13
14
15
16
17
18
19
20
21
22
23
24
25
26
27
28
29
30
31
32
33
34
35
36
37
38
39
40
41
42
43
44
45
46
47
48
49
50
51
52
53
54
55
56
57
58
59
60

Note: The following files were submitted by the author for peer review, but cannot be converted to PDF. You must view these files (e.g. movies) online.

Movie S1.mp4
Movie S2.mp4
Movie S3.mp4
Movie S1.avi
Movie S2.avi
Movie S3.avi

SCHOLARONE™
Manuscripts

Functional Contributions of Strong and Weak Cellular Oscillators to Synchrony and Light-Shifted Phase Dynamics

Logan Roberts[a*], Tanya L. Leise[b*], David K. Welsh[c,d], Todd C. Holmes[a**]

[*] Co-first authors

[a] Department of Physiology and Biophysics, University of California, Irvine, Irvine, CA, 92697;

[b] Department of Mathematics and Statistics, Amherst College, Amherst, MA 01002;

[c] Department of Psychiatry and Center for Circadian Biology, University of California, San Diego, La Jolla, CA 92093; [d] Veterans Affairs San Diego Healthcare System, San Diego, CA 92161.

[**] To whom correspondence should be addressed, email: tholmes@uci.edu

Running title: *Ex vivo* and *in silico* light-shifted phase dynamics of strong and weak oscillators.

Abstract: Light is the primary signal that calibrates circadian neural circuits and thus coordinates daily physiological and behavioral rhythms with solar entrainment cues. *Drosophila* and mammalian circadian circuits consist of diverse populations of cellular oscillators that exhibit a wide range of dynamic light responses, periods, phases, and degrees of synchrony. How heterogeneous circadian circuits can generate robust physiological rhythms while remaining flexible enough to respond to synchronizing stimuli has long remained enigmatic. Cryptochrome is a short wavelength photoreceptor that is endogenously expressed in approximately half of *Drosophila* circadian neurons. In a previous study, physiological light response was measured using real-time bioluminescence recordings in *Drosophila* whole brain explants which remain intrinsically light-sensitive. Here we apply analysis of real-time bioluminescence experimental data to show detailed dynamic ensemble representations of whole circadian circuit light entrainment at single neuron resolution. Organotypic whole brain explants were either maintained in constant darkness (DD) for 6 days or exposed to a phase advancing light pulse on the second day. We find that stronger circadian oscillators support robust overall circuit rhythmicity in DD, whereas weaker oscillators can be pushed toward transient desynchrony and damped amplitude to facilitate a new state of phase-shifted network synchrony. Additionally, we employ mathematical modeling to examine how a network composed of distinct oscillator types can give rise to complex dynamic signatures in DD conditions and in response to simulated light pulses. Simulations suggest that complementary coupling mechanisms and a combination of strong and weak oscillators may enable a robust yet flexible circadian network that promotes both synchrony and entrainment. A more complete understanding of how the properties of oscillators and their signaling mechanisms facilitate their distinct roles in light entrainment may allow us to direct and augment the circadian system to speed recovery from jet lag, shift work, and seasonal affective disorder.

Key words: Circadian, light, neural circuits, bioluminescence, phase dynamics, model simulations.

Introduction

Since the relatively recent advent of high speed flight and artificial lighting, a growing proportion of the human population suffers chrono-disruption due to mismatch between biological and environmental timing. Circadian disruption by events such as jet lag and shift work are implicated in physiological disorders ranging from decreased cognitive performance and weight gain to diabetes and cancer (Stevens and Rea, 2001; Lemmer, 2006; Knutson et al., 2007; Kreier et al., 2007; Maemura et al., 2007; Mazuski and Herzog, 2015). Circadian neural circuits coordinate and synchronize physiological and behavioral activities by integrating environmental cues. Light is the most powerful cue for most organisms (Pittendrigh and Daan, 1976; Tauber and Kyriacou, 2001). Light evoked changes in mammalian cellular oscillator dynamics is still largely unexplored due to the technical difficulty of introducing a physiological light signal *in vitro* (Evans et al., 2011; Foley et al., 2011; Webb et al., 2012). For the mammalian circadian pacemaker, the suprachiasmatic nucleus (SCN), physiologically activating retina-mediated photic responses while monitoring large numbers of deep brain individual cellular oscillators by imaging or electrophysiology remains a formidable challenge, both *ex vivo* and *in vivo*. However, in the *Drosophila* circadian system, circuit-wide responses to light can be monitored longitudinally in cultured whole brain explants (Ayaz et al., 2008; Roberts et al., 2015) due to expression of the blue light receptor Cryptochrome (CRY) in circadian neurons (Emery et al., 1998; Stanewsky et al., 1998; Fogle et al., 2011).

To examine dynamic signatures of single-neuron oscillators and their potential roles in entrainment, we analyzed and compared *ex vivo* and *in silico* single oscillator longitudinal light responses. *Ex vivo* analysis was based on real-time bioluminescence imaging of the conserved and critical circadian gene *period* in cultured *Drosophila* whole brain explants, as previously described (Roberts et al., 2015). Explants were either maintained in constant darkness for 6 days or exposed to a circadian-time 22 h (CT22) phase advancing white light pulse after nearly 2 days in culture. The *Drosophila* circadian network minimally consists of six neuronal subgroups that include large and small ventrolateral neurons (l-LNvs and s-LNvs), dorsolateral neurons (LNds), and three subsets of dorsal neurons (DNs 1, 2 and 3) (Sheeba, 2008). Recent studies have further subdivided these subgroups by chemical or genetic markers (Shafer et al., 2006; Hamasaka et al., 2007; Johard et al., 2009; Zhang et al., 2010a; Zhang et al., 2010b; Collins et al., 2012). Visualization and quantification of longitudinal changes in circadian network phase, amplitude, and synchrony with single oscillator resolution allows us to compare the contributions of different types of circadian oscillators to free-running behavior and light-induced phase shifts.

Motivated by the striking qualitative trends observed in the whole brain imaging data, we also developed a mathematical model of a relatively simple network consisting of three categories of oscillators with differing light responses, signaling mechanisms, and damping rates. The primary purpose of our model is to explore how and why complex dynamic signatures might emerge,

2

with distinct patterns appearing under constant conditions and in response to a strong phase advancing stimulus. It has long been recognized that robust and synchronous circadian networks are critical for strong and healthy behavioral outputs. However, our *ex vivo* findings and computational modeling suggest that transiently desynchronizing and damping certain components of the circadian neural network may be a key adaptive feature of circadian systems that facilitates large shifts in phase while restoring synchronous rhythmicity after the adjustment is complete. The combination of single-cell resolution imaging with mathematical modeling may allow us to predict how the dynamic interplay of complementary oscillatory types and transient desynchrony could be harnessed to generate potential treatments for jet lag, shift work, and seasonal affective disorder.

Materials and Methods

Experimental Bioluminescence Data

Adult, male *XLG-Per-Luc* flies were entrained to a standard 12 hr:12 hr LD schedule for ≥3 days. *Drosophila* whole brains were dissected, cultured, and mounted on the stage of an inverted microscope (Olympus IX71, Tokyo, Japan) as described (Roberts et al., 2015), with cycling bioluminescence at single cell resolution measured at 30 minute intervals by the software MetaMorph (Molecular Devices, Sunnyvale, CA). Whole brain explants were either maintained in constant darkness (DD) for 6 days (n=12) or exposed to a phase advancing 12.57 W/m^2 (2,000 lux), 15 minute white light pulse at CT 22 on the second day of DD (n=12).

Raster plots (Pseudo-Heat Maps)

Pseudo-heat maps of individual oscillator PER-luc expression over time in cultured *Drosophila* whole brain explants were generated using MATLAB scripts (version 8.2). Analysis of experimental data used throughout this study was based on bioluminescence imaging experiments reported previously (Roberts et al., 2015). Pseudo-heat maps were generated for each neuronal subgroup and also stacked for plots of "all cells." Warmer colors indicate higher amplitude whereas cooler colors indicate lower amplitude.

Circular Phase Plots (Sine Fit)

Circular phase plots were generated based on sine-fit estimates of wavelet detrended time series using the midpoint of 2-day sliding windows. Custom MATLAB scripts integrated the WMTSA wavelet Toolkit (C. Cornish, U. of Washington, WA) for application of a discrete wavelet transform to all data sets. These plots show the phases of individual oscillators categorized by neuronal subgroup as well as for "all cells" (combined across all subgroups from 12 brains). The circular plots display phases in terms of CT, with CT 0 set equal to the overall mean phase of "all cells" for Day 1. The inner circle shows the alpha = 0.05 threshold for the resultant vector for the Rayleigh test. The null hypothesis is that phases are uniformly distributed. If the resultant vector ends outside the inner circle then the phase distribution is significantly different from the uniform distribution. The absence of plots for certain time points indicates that the rhythmicity of

3

neurons in that subgroup at that time point was too dampened for reliable sine-fit measures (i.e. did not meet the criteria for "reliably rhythmic cells"). Oscillators were deemed reliably rhythmic if their good-of-sine-fit was greater than a threshold value of 0.82, their period was between 18h and 30h, and their amplitude was at least 1.5, as described in (Roberts et al., 2015).

Validation of Sine-Fit Estimates

To verify that single oscillator phases were reliably extracted through sine-fits of the wavelet detrended time series, circular phase plots were also generated using a time delay embedding method. Briefly, the time series were embedded in a higher dimension via lagging by 6 hours so that oscillations circle the origin; see *Nonlinear Time Series Analysis 2nd Edition* by H. Kantz and T. Schreiber (Cambridge University Press, 2003) for details on time delay embedding. The polar angle was then used as a phase estimate. As with the sine-fit estimates, phases are displayed in terms of CT, with CT 0 set equal to the overall mean phase of "all cells" for Day 1. Phase plots generated using 2-dimensional embedded phase analysis showed the same patterns of oscillator activity as plots generated using sine-fit estimates. MATLAB scripts were used to calculate the correlation coefficients (rho) and p-values between the time delay embedding estimates and the sine-fit phase estimates across all neuronal subgroups for all time points and conditions. The p-value is based on the null hypothesis that there is no correlation in phase estimates between these two methods. The strong positive, linear correlation (indicated by high rho values) and low p-values in Table S1 confirm that sine-fit estimates of phase using two-day sliding windows are sufficiently reliable and consistent. The same neurons were analyzed for both methods for corresponding time points, subgroups, and conditions.

Calculation of Order Parameter

To quantify changes in synchrony over time, we use the order parameter R, defined as in (Gonze et al., 2005) for a system of N oscillators with state variable X:

$$R = \frac{\langle X^2 \rangle - \langle X \rangle^2}{\frac{1}{N} \sum_{k=1}^{N} \left(\langle X_k^2 \rangle - \langle X_k \rangle^2 \right)},$$

where angle brackets denote time average and $X = \frac{1}{N} \sum_{k=1}^{N} X_k$. If the phase, period and waveform of all N cells are in perfect synchrony then $R=1$, while a uniform distribution of phases would lead to $R=0$.

Phase Ensemble Animations

Custom MATLAB scripts were used to generate phase ensemble animations based on bioluminescence experimental data comparing changes in phase and amplitude over time among oscillators of brain explants either maintained in constant darkness or exposed to a phase advancing white light pulse as described (Roberts et al., 2015). The phase of each oscillator is

4

represented by the polar angle of the disks, whereas amplitude is indicated by the radial distance of the disks from the center of the circle (drift towards the center indicates damping amplitude). The animations were generated using custom MATLAB scripts with estimates of phase and amplitude calculated using 2-dimensional embedding applied to wavelet-detrended traces. Phase and amplitude dynamics are shown at three levels of resolution: single neuron oscillators (Supp. Movie 1), individual neuronal subgroups (Supp. Movie 2), and whole network (Supp. Movie 3).

Model Simulations

Mathematical modeling was performed using custom MATLAB scripts to explore the qualitative emergent dynamic behaviors of a network composed of different oscillator types, based on current knowledge of what we expect to be present in the *Drosophila* circadian network. This model provides a simplified negative feedback loop, roughly mimicking that of the circadian transcriptional-translational feedback loop, while remaining simple enough for an exact stability analysis (Tyson 2002). The model is built on three types of oscillators with distinct types of signaling, light responses, and degrees of dampening. However, they are not meant to specifically represent particular neuronal subgroups or neurotransmitters. The main premise is to demonstrate through a relatively simple model how different dynamic signatures could be generated and how these could be advantageous to the circadian system.

Each oscillator is simulated using a modified version of the Goodwin model (Bliss et al., 1982; Tyson, 2002) which consists of three differential equations forming a negative feedback loop:

$$\frac{dX}{dt} = \frac{a(1 + k_{act} - k_{rep})}{Z + 1} - bX \quad (1)$$

$$\frac{dY}{dt} = bX - bY \quad (2)$$

$$\frac{dZ}{dt} = bY - \frac{cZ}{Z + 1} \quad (3)$$

The parameters are set so that oscillations dampen toward steady state values over time (see Table 1):

$$X_{ss} = Y_{ss} = \frac{a}{b(1 + a/c)} \text{ and } Z_{ss} = \frac{a}{c}.$$

Although the individual oscillators are damped, the coupled system described below generates sustained oscillations for $\beta > 0.03$ under constant conditions, and also entrains to light-dark cycles. See Fig. M1-4 in the Mathematical Modeling Supplement.

	s	a	b	c	β
Group 1	0.98±0.005	$(9s-1)c$	0.149-0.1535	$81bs^2$	0.035±0.007

| Group 2 | 0.98±0.005 | $(9s-1)c$ | 0.1525-0.157 | $81bs^2$ | 0.035±0.007 |
| Group 3 | 0.88±0.005 | $(9s-1)c$ | 0.149-0.157 | $81bs^2$ | 0.175±0.035 |

Table 1. Parameter values for Goodwin model. The model generates self-sustained oscillations in individual oscillators if $s>1$ and damped oscillations if $s<1$ (with smaller s leading to faster damping). To create heterogeneity in the oscillator groups, values of s and β are normally distributed random numbers with the indicated mean and standard deviation, while values for b are evenly distributed in the indicated range for each group (not random). Parameters a and c are fixed functions of s and b; see (Tyson, 2002) for the derivation of these relations via a linear stability analysis. Group 3 needs a stronger coupling signal to maintain rhythmicity, due to its low value of s (strongly damped).

To explore the dynamic interactions of damped oscillators with different properties, we created a network of 60 Goodwin oscillators organized into 3 groups. "Group 1" oscillators (10 total, #1-10) are directly light responsive, weakly damped, and send an activating coupling signal that effectively increases the transcription rate a of all oscillators when the Group 1 oscillators have X levels above the theoretical steady state value X_{ss}. "Group 2" oscillators (10 total, #11-20) are more strongly light responsive, weakly damped, and transmit a repressing coupling signal that effectively decreases the transcription rate a of all oscillators when the Group 2 oscillators have Z levels above the steady state value Z_{ss}. These coupling functions were chosen to appropriately time the signals to promote synchronization. In both cases, higher amplitude oscillations lead to stronger coupling. "Group 3" oscillators (40 total, #21-60) are not directly light responsive, strongly damped, and send a repressing coupling signal similar to that of Group 2.

Light response is achieved through increasing the degradation rate parameter c in equation (3). Both LD entrainment and response to light pulses can be effectively modeled through this mechanism. For example, a light pulse simulated by increasing c by 8% for Group 1 oscillators and by 16% for Group 2 oscillators for 4 hours starting 3 hours before the peak in mean X results in a large phase advance of nearly 9h for the coupled system. LD entrainment can be simulated by increasing c by 0.4% for Group 1 oscillators and by 0.8% for Group 2 oscillators for the first 10h of each 24h day.

Coupling is achieved through modifying the transcription rate parameter a as indicated in equation (1). Two complementary types are used for the modeling: k_{act} increases transcriptional activation while k_{rep} represses transcription in equation (1):

$$k_{act} = \frac{\beta}{10} \sum_{n=1}^{10} \frac{\max(X_n - X_{ss}, 0)}{X_{ss} + \max(X_n - X_{ss}, 0)},$$

6

$$k_{rep} = \frac{\beta}{50} \sum_{n=11}^{60} \frac{\max(Z_n - Z_{ss}, 0)}{Z_{ss} + \max(Z_n - Z_{ss}, 0)} \, .$$

All oscillators receive both types of coupling signals, but each group sends a single type of coupling signal. Note that in the alternate simulations where only one type of coupling is used, then all 3 groups send the indicated type of signal (activating or repressing). See the Mathematical Modeling Supplement for further details.

Results

Drosophila circadian neuronal subgroups exhibit distinct dynamic signatures in constant darkness and in response to a phase advancing light pulse

A longstanding question in circadian biology has been to discern which aspects of circadian rhythm dynamics and light entrainment are due to the relative contributions of cell autonomous and network properties (Liu et al., 2007; Yan et al., 2007; Sheeba et al., 2008; Wang et al., 2008). Real-time bioluminescence recordings have previously shown that oscillators in cultured *XLG-Per-Luc* whole brain explants maintained in constant darkness exhibit a monotonic decrease in amplitude and synchrony (**Fig. 1A, Supp. Fig. 1**) (Roberts et al., 2015). In contrast, perturbation of neuronal subgroups with a 12.57 W/m^2 (2,000 lux) 15 minute phase advancing white light pulse evokes transient loss of synchrony and amplitude with subsequent recovery of phase-shifted synchrony over time through the process of "phase retuning" (**Fig. 1A**). The heterogeneity of phase, period, amplitude, synchrony and light response for each of the neuronal subgroups is qualitatively apparent in raster heat map plots based on bioluminescence reporting of *period* activity (**Fig. 1B**). However, questions remain concerning how such a heterogeneous system may arise and how it may be advantageous for circadian behavior and entrainment.

Drosophila heterogeneous circadian neural networks are robust but flexible

Cellular circadian oscillators found in the *Drosophila* circadian network and the mammalian suprachiasmatic nucleus (SCN) are known to exhibit a wide range of periods, phases, amplitudes and signaling properties (Peng et al., 2003; Quintero et al., 2003; Schaap et al., 2003; Yamaguchi et al., 2003). To increase our understanding of the roles played by different components of the circadian network, we examined how phase relationships are transiently altered during environmental adaptation. As a basis for comparison, we first observed phase relationships under constant conditions by performing quantified spatiotemporal mapping of single oscillator phase dynamics using sine-fit phase estimates for cultured adult *Drosophila* whole brain explants maintained in constant darkness (DD) for 6 days (Roberts et al., 2015). The results indicate that circadian networks consisting of oscillators with a wide range of intrinsic phases and periods are still capable of maintaining consistent mean network phase and robust phase synchrony as shown by the phase angle at or very close to CT0 over time in the

7

absence of perturbation by environmental cues (**Fig. 2A, Top Row**). This remarkably consistent network phase relationship is highly robust in the whole brain preparation as show by little deviation of the phase vector angle for all oscillators from CT 0 over multiple days. However, the circadian neural network is also capable of a strong response when stimulated with a 15 minute phase advancing light pulse (LP) at CT 22 of the second day in DD, which evokes transient phase dispersion followed by resynchronization of phase-shifted oscillators (**Fig. 2A, Bottom Row**).

To examine the emergent roles of individual neuronal subgroups, we compared subgroups' mean phases and amplitudes in **Figure 2B**. Neuronal subgroups as a whole are considered to have significant desynchrony or damped amplitude at any time point if the mean output phase cannot be measured. This is qualitatively apparent by the absence of a color-coded disc representing a subgroup's mean phase because no phase estimates can be reliably calculated as the phase coherence and/or amplitude is too low (**Fig. 2B**). In this study, we describe oscillators as "weak" or "strong" based on the robustness of their free-running activity in DD. As the s-LNvs and LNds are the only neuronal subgroups to exhibit robust phase coherence throughout recordings, they are considered stronger neuronal subgroups (**Fig. 2B**). Conversely, the DN3s, DN1s and l-LNvs are considered weaker oscillators as they exhibit significant desynchrony and/or damped amplitude by the end of the recordings in DD. By comparing inter-neuronal subgroup dynamics, we observe that the s-LNvs are the only subgroup to maintain a robust and consistent mean phase near CT 0 throughout the recordings. Interestingly, the s-LNvs exhibit the most rapid phase dispersion and damped amplitude in response to the phase advancing light pulse. Another pivotal subgroup is the LNds, the only subgroup to maintain phase coherence and exhibit a high fidelity rapid phase shift of 2 hours (**Supp. Fig. 2**) by Day 3 after the LP. This analysis shows that the LNds did not just begin to shift on Day 3, which is observed to a lesser extent in the DN3s and s-LNvs, but immediately achieved the large final phase shift. This provides evidence that the LNds are not just first responders, but likely have a more important role in pulling the network to the new phase state. Conversely, the amplitude and phase coherence of all other subgroups are transiently suppressed following the light pulse. Snapshots of animations of bioluminescence experimental data from **Supp. Movie 1** of single oscillator phase ensembles over time are shown to demonstrate the complexity and diverse range of oscillator activities in DD and in response to the LP (**Fig. 2C**). In order to more clearly compare complex cell autonomous and whole network dynamics in DD and in response to a phase advancing light pulse, we generated dynamic movie animations of oscillator phase ensembles based on quantified bioluminescence data at three degrees of resolution: single neuron (**Supp. Movie 1, discs color coded by neuronal subgroup**), individual neuronal subgroup (**Supp. Movie 2, discs color coded by neuronal subgroup**), and whole network average (**Supp. Movie 3**). These movies convey the complexity of quantified circadian oscillators' dynamics and allow for clearer simultaneous, longitudinal comparisons of circadian network activity. Movie 1, showing single oscillator resolution, demonstrates how oscillator dynamics within and between subgroups would be practically impossible to discern using the standard static measures such as

8

immunocytochemistry. These results motivated us to map the complex phase dynamics and explore their potential impacts on endogenous rhythms and response to light cues.

Quantification of neuron subgroups' phases in constant darkness reveals complementary inter-subgroup free-running phase dynamics

Studies suggest that dynamic changes in phase relationships and synchrony among autonomous oscillators distributed throughout a circadian circuit can generate distinct physiological outputs such as seasonal adaption (Inagaki et al., 2007; Stoleru et al., 2007; Coomans et al., 2015a; Coomans et al., 2015b). By quantifying individual oscillator phase and overall subgroup phase coherence, we mapped the distinct dynamic signatures of neuron subgroups in whole brain explants maintained in constant darkness (**Fig. 3**). As previously described, most subgroups exhibit a monotonic decrease in rhythmic strength and phase coherence over time in DD (Roberts et al., 2015). We observe that the s-LNvs, which are considered the core pacemaker neurons (Yang and Sehgal, 2001; Shafer et al., 2002; Helfrich-Förster, 2003), appear to have the most strongly coherent and consistent phases in DD relative to other subgroups (**Fig. 3**). More importantly, the s-LNvs are the only subgroup that exhibits a robust and consistent mean phase with a phase angle very close to CT 0 that approximates the overall network's mean phase over time (compare **Supp. Movies 2 and 3**). This indicates that the s-LNvs may have a predominant role in maintaining free-running rhythms over time in DD. Similarly, weaker oscillators such as the DN1s and DN3s exhibit relatively consistent mean phases with phase angles very close to CT 0 but relatively greater phase dispersion than the s-LNv after 3-4 days in DD. Intriguingly, the l-LNvs and LNds exhibit coherent but nearly opposite phase relationships over time so that the mean network phase is still consistently maintained near CT 0. The consistency of the overall mean network phase remains robust in spite of the increased spread of single oscillators' phases over time, suggesting that even free-running activity is not merely stochastic but remains measurably coordinated at the network level. The next step was to observe how these relationships might change following the application of a phase advancing light pulse to *Drosophila* whole brain explants.

A light-evoked phase shift pushes most oscillators towards quantitative transient desynchrony and damped amplitude before the network adopts a new state of phase-shifted synchrony

The physiological importance of robust, coordinated and consistent circadian oscillations has long been recognized. However, recent studies and models have revealed that more complex dynamics of synchrony and single oscillator activities may underlie circadian adaptations to events such as seasons, travel across time zones, and shift work (Schaap et al., 2003; Leise and Siegelmann, 2006; Stoleru et al., 2007; An et al., 2013; Muraro et al., 2013; Coomans et al., 2015b; Roberts et al., 2015). To examine the response of the circadian network to light more closely, we measured the intricate spatiotemporal phase dynamics of individual oscillator responses to a phase advancing light pulse (**Fig. 4**). Intriguingly, the strong s-LNvs, which

9

exhibit the most robust rhythms over time in DD, conversely exhibit the most rapid phase dispersion following the LP on day 2 and do not recover significant phase coherence until day 4. However, it should be noted the mean phase shift achieved by the s-LNvs on day 5 most closely approximates the final mean phase shift achieved by the overall network (compare **Fig. 2A** to **Fig. 4**). In contrast, oscillators which exhibit generally weaker free-running oscillations, such as the DN3s and DN1s, maintain relatively greater intra-subgroup phase coherence immediately following the light pulse on Day 2 but exhibit significant loss of phase coherence by day 3. The DN3s do not express Cry and are thus not directly photosensitive. However, the DN3s exhibit a more immediate mean phase advance compared to the stronger s-LNvs. The small but immediate light-evoked phase shift observed in the "light blind" DN3s indicates that the neural connections in the organotypic whole brain explants are still sufficiently intact for communication from the Cry-expressing circadian neurons. However, it should be noted that the DN3s also exhibit the smallest mean phase shift by the end of the recordings. As observed in DD, the l-LNvs and LNds exhibit a seemingly complementary relationship in which the l-LNvs show significant dampening of rhythmicity by Day 3 following the light pulse, whereas the LNds show an increase in phase coherence by Day 3 following the light pulse (**Supp. Figs. 2 and 3**). The LNds are the first subgroup to complete the phase shift, achieving a large phase advance by Day 3 (**Fig. 4, Supp. Fig. 3**).

To verify that single oscillator phases were reliably extracted though sine-fit estimates of wavelet detrended time series, we also calculated oscillator phases in DD (**Supp. Figs. 4 and 5**) and in response to the LP (**Supp. Fig. 6**) using a 2-dimensional time delay embedding method (see Supplemental Information for details). The strong, positive correlation in phase estimates between the sine-fit and time delay embedding phase methods confirms that quantified trends of dynamic oscillator activity in both light conditions and across all subgroups are reliable and consistent (**Supp. Table 1**). The complex and distinct dynamics exhibited by these neuronal subgroups motivated us to use mathematical modeling to explore what network and oscillator properties may generate these dynamics and the potential benefits.

Mathematical modeling of circadian network dynamics demonstrates potential benefits of complementary coupling and a mix of strong and weak oscillators

To study the key features leading to the complex emergent dynamics observed in the experimental oscillator relationships, we developed a relatively simple mathematical model of a coupled network of 60 oscillators based on a modified Goodwin model (Tyson, 2002). The oscillators are divided into three groups with differing light responses, inhibitory versus excitatory coupling signal, and oscillator damping rate. These features are based on our current ideas about qualitative features of the *Drosophila* circadian circuit guided by the literature (Collins et al., 2014; Dissel et al., 2014; Yao and Shafer, 2014) and our own experimental data. "Group 1" oscillators (10 total) are moderately light responsive, weakly damped, and send a phased coupling signal that effectively increases the transcription rate of all oscillators. "Group 2" oscillators (10 total) are strongly light responsive, weakly damped, and transmit a coupling

10

signal that effectively decreases the transcription rate of all oscillators. The timing of the activating and repressing coupling signals were chosen to be nearly antiphase to each other in order to promote synchronization. "Group 3" oscillators (40 total) are not light responsive, are strongly damped, and send a repressing coupling signal similar to that of Group 2. See the Methods and the Mathematical Modeling Supplement for a complete description of the model. Note that the model is not meant to directly represent particular neuronal subgroups or neurotransmitters, as we lack sufficient knowledge to create a detailed model at this time. The model simulations reproduce many of the general emergent patterns of free-running behavior and light response observed in our empirical data (**Fig. 5A-C**). In DD simulations, we observe a monotonic decrease in amplitude and synchrony for all groups, with the Group 1 oscillators maintaining relatively high amplitude, synchronous oscillations in the absence of perturbations. In contrast, a simulated phase advancing light pulse transiently suppresses the amplitudes and scrambles the phases of oscillators in Groups 1 and 3, followed by a delayed recovery and strengthening of both amplitude and phase coherence relative to corresponding oscillators in the DD condition. Note that Group 2 oscillators display an immediate increase in amplitude and phase synchrony in response to the light pulse and push the network towards a new state of phase-shifted synchrony.

To explore the potential benefits of complementary coupling, we also performed simulations with "activating only" coupling, in which all oscillators send coupling signals that increase transcription, and "repressing only" coupling, in which all oscillators send coupling signals that decrease transcription (**Fig. 5D-E**). The equations and parameters for these contrasting models are identical apart from the differences in coupling. "Activating only" coupling results in a lower order parameter R and reduced magnitude of phase shifts as shown on the simulated phase response curve (**Fig. 5D**) and also a reduced phase advance in response to the 4h light pulse (Fig. M5-6 in the Mathematical Modeling Supplement). Furthermore, these oscillators have a longer overall period of 24.3 hours in DD compared to a period of 23.9 hours in DD for the mixed coupling model (**Fig. 5E**). On the other hand, "repressing only" coupling results in a slightly shorter overall period of 23.7 hours in DD and somewhat larger phase shifts (**Fig. 5DE;** see also Fig. M3 in the Mathematical Modeling Supplement). Furthermore, the "repressing only" coupling can be less stable in terms of greatly increased responses to light pulses if the coupling strength is decreased, compared to the cases of "activating only" and mixed coupling (**Fig. M9-11** in the Mathematical Modeling Supplement). One benefit of the complementary coupling mechanisms is that increasing the coupling strength minimally effects the system's period while greatly increasing the overall synchronization and amplitude, as shown in Figs. M3-4. This allows for adaptive changes in phase coherence and amplitude with only slight changes to the period. The period itself may be adjusted by altering the balance between activating and repressing coupling, which tend to respectively lengthen and shorten the period.

As shown in Figs. M12-15 in the Mathematical Modeling Supplement, the system exhibits a higher order parameter R when the system contains both weaker and stronger oscillators

11

(indicating that the system is more easily synchronized), and the weaker oscillators are also necessary for the advancing light pulse to cause a transient dip in R followed by an overshoot. However, too great of a damping rate in the weaker oscillators will reduce the overall coherence of the system, as shown in Fig. M16. Thus the presence of both stronger and weaker oscillators appears to play a key role in the dynamics of the system.

Discussion

The present study combines *ex vivo* experimental bioluminescence data with *in silico* model simulations to provide evidence for how circadian networks with a mix of strong and weak oscillators and complementary coupling mechanisms may contribute to robust yet responsive oscillations. Due to an increasing awareness of the detrimental effects of chronodisruption by common environmental events and features such as jet lag, shift work, and late night screen viewing time, numerous investigators have examined the importance of consistent and synchronized rhythms (Colwell et al., 2003; Yamaguchi et al., 2003). However, recent studies have shown that desynchrony is not always pathological and even varies between seasons (Schaap et al., 2003; Herzog et al., 2004; Stoleru et al., 2007; An et al., 2013; Hastings et al., 2014; Coomans et al., 2015b; Roberts et al., 2015). Using custom analysis of real-time bioluminescence datasets, we show the first detailed spatiotemporal mapping of dynamic phase relationships within an entire circadian neural circuit, at single neuron resolution, both in DD and in response to a light pulse. The complexity of multiday single oscillator phase dynamics revealed here underlines the difficulty in understanding biological clocks by cross-sectional methods such as immunocytochemistry or acute electrophysiology, and the importance of longitudinal analysis of single-cell circadian rhythms by methods such as whole brain bioluminescence imaging.

Accordingly, we endeavored to quantify and map the spatiotemporal dynamics of oscillators in whole *Drosophila* brain explants either maintained in constant darkness (DD) or exposed to a phase advancing light pulse (LP). Although recent studies have further subdivided the *Drosophila* circadian circuit based on neuropeptide or genetic markers (Veleri et al., 2003; Gonze et al., 2005; Nitabach and Taghert, 2008; Zhang et al., 2010a; Zhang et al., 2010b; Collins et al., 2012), analysis in this study was limited to the classical anatomically recognized s-LNv, l-LNv, LNd, DN1 and DN3 subgroups. Future studies will functionally dissect further subdivisions of the circuit. Numerous studies have investigated how the intrinsic and heterogeneous activities of autonomous single-cell oscillators distributed throughout circadian circuits map to daily behavioral rhythms and entrainment. Sub-regions of the SCN have been shown to have a diverse range of periods, phases, and dynamics of light response (Evans et al., 2011; Foley et al., 2011). In this study, we confirm that, even in the absence of perturbation by external cues, different components of the *Drosophila* circadian circuit display a wide range of intrinsic oscillator phases, periods, and phase coherence. Interestingly, the heterogeneous

circadian oscillators have complementary activities in whole brain explants maintained in DD so that the network has a whole still exhibits a remarkably robust and consistent overall mean phase over time in spite of the increase spread in oscillators' periods and phases over time. This indicates that the activity of these heterogeneous groups does not merely become stochastic in DD, but that their phases remain coordinated to some extent. The stability and coherence of oscillator phases over time in DD also further supports the robustness and utility of cultured *XLG-Per-Luc* whole brain explants. We observe that the s-LNvs, which exhibit strongly consistent and coherent free-running rhythms, have a mean phase that most closely matches the overall network mean phase for all 6 days of recording. Though the weaker DN1s and DN3s also show a relatively consistent mean phase over time, they exhibit more rapid damping of amplitude and phase dispersion over time. The LNds and l-LNvs also exhibit coherent phases over time in DD but do not maintain a consistent mean phase near CT 0. This supports previous studies indicating that the s-LNvs have key roles as pacemaker neurons (Yang and Sehgal, 2001; Shafer et al., 2002; Helfrich-Förster, 2003). However, the mean phase of the circuit as a whole also appears to be generated by the complementary dynamics of the fast-paced (<24 hour period) l-LNvs and slow-paced (>24 hour period) LNds. Although these subgroups both exhibit significant and coherent phase drift in DD, the network mean phase is maintained due to the nearly exact mirroring of their opposite phase drifts over time. The complementary activities of the l-LNvs and LNds agree with previous findings of slow-paced and fast-paced oscillators (Dissel et al., 2014). This is intriguing, as these two subgroups also appear to have complementary responses to a phase-advancing light pulse, in which the LNds exhibit an immediate increase in amplitude and phase coherence whereas the l-LNvs show an immediate decrease in amplitude and phase coherence. The complementary activities of the LNds and l-LNvs in DD and in response to a phase advancing light pulse suggest that the l-LNvs and LNds may play unique roles in circadian network responses to cues of different phases. We also emphasize the potential roles of the weaker DN1s and DN3s which recover synchrony much more quickly than the stronger s-LNvs following exposure to the light pulse. This agrees with previous work indicating that weaker oscillators can adjust their phase more readily and enhance resynchrony (Webb et al., 2012). These findings suggest that certain cells may intrinsically maintain more stable phases for supporting robust free-running circadian rhythms, whereas more weakly circadian cells may have faster or slower intrinsic rhythms to enable more flexible adaptation to environmental changes.

The dual importance of the strength of circadian rhythms along with plasticity of circadian networks to enable adaptation to various environmental cues are critical feature. By combining single-cell phase dynamic analysis of *ex vivo* whole circuit bioluminescence experimental data with computational modeling of emergent network dynamics, we provide evidence that transiently desynchronizing and damping most oscillators in a neural network may actually be a key feature for facilitating entrainment by light for the whole circuit. We postulate that a phase advancing light pulse at CT 22 scrambles most oscillators' phases and suppresses amplitudes so that stronger oscillators such as the LNds, which exhibit an increase in phase coherence and

13

amplitude, can lead the rest of the transiently weakened network towards a new state of phase-shifted synchrony. Although altering oscillators' phase coherence or amplitudes may have different downstream consequences, we observe that dynamic changes in coherence and amplitude appear to coincide in response to the phase advancing light pulse. This is also important for the mammalian SCN for which the phase and amplitude of coupling for both damped and sustained oscillators have been shown to be critical for synchrony and entrainment (Ananthasubramaniam et al., 2014). Thus, there is precedent for this coupling paradigm in circadian models.

In both the DD and LP conditions, we observe that there is always at least one group of strong oscillators, such as the s-LNvs and LNds, which appear to contribute to maintaining robust network mean phase over time. We previously showed that the LNds have an unexplained increase in phase coherence by the end of the recording following a phase advancing light pulse (Roberts et al., 2016). However, our new analysis here shows that the LNds exhibit an immediate increase in phase coherence and amplitude following the LP that coincides with their phase advance. Our mathematical modeling suggests that this increase in amplitude may be critical for shifting the rest of the network into a new advanced phase. Although the LNds exhibit the most immediate phase shift and increase in amplitude followed the LP, we note that the phase shift achieved by the s-LNvs on Day 5 most closely approximates the mean network phase shift on Day 5. This suggests that although the LNds appear to lead the phase shift, the new state of phase-shifted network synchrony is not achieved for behavioral output until other circuit elements such as the s-LNvs contribute to the ensemble output. This indicates that both these strong oscillator groups may have distinct contributions for the emergent behavioral output in response to the phase advancing light pulse. Though the weaker DN1s and DN3s maintained relatively consistent, but less coherent mean phase in DD, a phase advancing light pulse appears to transiently desynchronize and dampen their rhythms so that strong oscillators can drive the network toward the new state of phase shifted synchrony. We observe that the DN3s, which are not directly light-sensitive, show a more immediate coherent phase shift than any other subgroup except the LNds. However, the DN3s subsequently exhibit the most gradual phase shift that does not reach the mean network phase shift by the end of the recordings. These findings support previous studies indicating that transiently weakening oscillator coupling and rhythmicity may enable circuits to more easily adapt to phase shifts, whereas networks that are too rigid and fixed may have reduced entrainment capacities (Tsumoto et al., 2011; Webb et al., 2012; An et al., 2013; Freeman et al., 2013; Yamaguchi et al., 2013; Hatori et al., 2014; Lamba et al., 2014; Roberts et al., 2015).

Our computational modeling allowed us to explore the potential roles of complementary coupling mechanisms in producing the key features of the distinct dynamic signatures observed in our experimental imaging. Although this is a relatively simple model derived from general circadian trends observed in previous literature and our own experimental data, previous studies have shown that varying just a few key parameters can reproduce experimentally observed

14

circadian features (Tokuda et al., 2005). Our model simulations demonstrate how a complementary system of mixed signaling may enable robust but flexible period length, amplitude, synchrony and capacity for large phase shifts. These simulations agree with previous experimental and modeling studies which showed that complementary excitatory and inhibitory interactions between faster-paced and slower-paced neuronal oscillators allow for fine-tuning of emergent period and phase (Sheeba et al., 2008; Dissel et al., 2014; Yao and Shafer, 2014; DeWoskin et al., 2015). Our modeling also suggests that adjusting the balance between coupling types may enable either more robust rhythms or greater network adaptability to environmental cues.

By combining quantitative single oscillator phase dynamics analysis of *ex vivo* whole circuit bioluminescence experimental data with mathematical modeling of complementary oscillator types, we provide evidence that stronger circadian neurons contribute to maintaining robust rhythms whereas weaker oscillators confer the flexibility to respond to environmental cues by large phase advances. However, it is still unclear how the complex phase relationships found among oscillators across and even within neuronal subgroups precisely map to circadian behavior and entrainment. Further research is also necessary to assess the precise interplay of neurochemical and/or gene signaling during a light-evoked phase shift that increases the amplitude of certain oscillators such as the LNds but may push other oscillators toward a transient state of desynchrony and damped amplitude. Future studies may incorporate pharmacological and genetic targeting of network coupling between stronger and weaker oscillators to explore how this dynamic process may be induced, amplified, and harnessed to treat conditions such as jet lag, shift work and seasonal affective disorder.

References

An S, Harang R, Meeker K, Granados-Fuentes D, Tsai CA, Mazuski C, Kim J, Doyle FJ, Petzold LR, and Herzog ED (2013) A neuropeptide speeds circadian entrainment by reducing intercellular synchrony. Proceedings of the National Academy of Sciences 110:E4355-E4361.

Ananthasubramaniam, B., Herzog, E. D., & Herzel, H. (2014). Timing of neuropeptide coupling determines synchrony and entrainment in the mammalian circadian clock. PLoS Comput Biol, 10(4), e1003565.

Ayaz D, Leyssen M, Koch M, Yan J, Srahna M, Sheeba V, Fogle KJ, Holmes TC, and Hassan BA (2008) Axonal injury and regeneration in the adult brain of *Drosophila*. The Journal of Neuroscience 28:6010-6021.

Bliss RD, Painter PR, and Marr AG (1982) Role of feedback inhibition in stabilizing the classical operon. Journal of Theoretical Biology 97:177-193.

15

Collins B, Kane EA, Reeves DC, Akabas MH, and Blau J (2012) Balance of activity between LNvs and glutamatergic dorsal clock neurons promotes robust circadian rhythms in *Drosophila*. Neuron 74:706-718.

Collins B, Kaplan HS, Cavey M, Lelito KR, Bahle AH, Zhu Z, Macara AM, Roman G, Shafer OT, and Blau J (2014) Differentially Timed Extracellular Signals Synchronize Pacemaker Neuron Clocks.

Colwell CS, Michel S, Itri J, Rodriguez W, Tam J, Lelievre V, Hu Z, Liu X, and Waschek JA (2003) Disrupted circadian rhythms in VIP-and PHI-deficient mice. American Journal of Physiology-Regulatory, Integrative and Comparative Physiology 285:R939-R949.

Coomans C, Lucassen E, Kooijman S, Fifel K, Deboer T, Rensen P, Michel S, and Meijer J (2015a) Plasticity of circadian clocks and consequences for metabolism. Diabetes, Obesity and Metabolism 17:65-75.

Coomans CP, Ramkisoensing A, and Meijer JH (2015b) The suprachiasmatic nuclei as a seasonal clock. Frontiers in neuroendocrinology 37:29-42.

DeWoskin D, Myung J, Belle MD, Piggins HD, Takumi T, and Forger DB (2015) Distinct roles for GABA across multiple timescales in mammalian circadian timekeeping. Proceedings of the National Academy of Sciences 112:E3911-E3919.

Dissel S, Hansen CN, Özkaya Ö, Hemsley M, Kyriacou CP, and Rosato E (2014) The logic of circadian organization in *Drosophila*. Current Biology 24:2257-2266.

Emery P, So WV, Kaneko M, Hall JC, and Rosbash M (1998) CRY, a *Drosophila* clock and light-regulated cryptochrome, is a major contributor to circadian rhythm resetting and photosensitivity. Cell 95:669-679.

Evans JA, Leise TL, Castanon-Cervantes O, and Davidson AJ (2011) Intrinsic regulation of spatiotemporal organization within the suprachiasmatic nucleus.

Fogle KJ, Parson KG, Dahm NA, and Holmes TC (2011) CRYPTOCHROME is a blue-light sensor that regulates neuronal firing rate. Science 331.6023: 1409-1413.

Foley NC, Tong TY, Foley D, LeSauter J, Welsh DK, and Silver R (2011) Characterization of orderly spatiotemporal patterns of clock gene activation in mammalian suprachiasmatic nucleus. European Journal of Neuroscience 33:1851-1865.

Freeman GM, Krock RM, Aton SJ, Thaben P, and Herzog ED (2013) GABA networks destabilize genetic oscillations in the circadian pacemaker. Neuron 78:799-806.

Gonze D, Bernard S, Waltermann C, Kramer A, and Herzel H (2005) Spontaneous synchronization of coupled circadian oscillators. Biophysical Journal 89:120-129.

Hamasaka Y, Rieger D, Parmentier ML, Grau Y, Helfrich-Förster C, and Nässel DR (2007) Glutamate and its metabotropic receptor in *Drosophila* clock neuron circuits. Journal of Comparative Neurology 505:32-45.

Hastings M, Brancaccio M, and Maywood E (2014) Circadian pacemaking in cells and circuits of the suprachiasmatic nucleus. Journal of neuroendocrinology 26:2-10.

Hatori M, Gill S, Mure LS, Goulding M, O'Leary DD, and Panda S (2014) Lhx1 maintains synchrony among circadian oscillator neurons of the SCN. Elife 3:e03357.

Helfrich-Förster C (2003) The neuroarchitecture of the circadian clock in the brain of *Drosophila* melanogaster. Microscopy research and technique 62:94-102.

Herzog ED, Aton SJ, Numano R, Sakaki Y, and Tei H (2004) Temporal precision in the mammalian circadian system: a reliable clock from less reliable neurons. Journal of biological rhythms 19:35-46.

16

Inagaki N, Honma S, Ono D, Tanahashi Y, and Honma K-i (2007) Separate oscillating cell groups in mouse suprachiasmatic nucleus couple photoperiodically to the onset and end of daily activity. Proceedings of the National Academy of Sciences 104:7664-7669.

Johard HA, Yoishii T, Dircksen H, Cusumano P, Rouyer F, Helfrich-Förster C, and Nässel DR (2009) Peptidergic clock neurons in *Drosophila*: ion transport peptide and short neuropeptide F in subsets of dorsal and ventral lateral neurons. Journal of Comparative Neurology 516:59-73.

Knutson KL, Spiegel K, Penev P, and Van Cauter E (2007) The metabolic consequences of sleep deprivation. Sleep medicine reviews 11:163-178.

Kreier F, Kalsbeek A, Sauerwein HP, Fliers E, Romijn JA, and Buijs RM (2007) "Diabetes of the elderly" and type 2 diabetes in younger patients: Possible role of the biological clock. Experimental gerontology 42:22-27.

Lamba P, Bilodeau-Wentworth D, Emery P, and Zhang Y (2014) Morning and evening oscillators cooperate to reset circadian behavior in response to light input. Cell reports 7:601-608.

Leise T, and Siegelmann H (2006) Dynamics of a multistage circadian system. Journal of biological rhythms 21:314-323.

Lemmer B (2006) Importance of Circadian Rhythms for Regulation of the Cardiovascular System-Studies in Animal and Man. In Engineering in Medicine and Biology Society, 2006 EMBS'06 28th Annual International Conference of the IEEE, pp 168-170, IEEE.

Liu AC, Welsh DK, Ko CH, Tran HG, Zhang EE, Priest AA, Buhr ED, Singer O, Meeker K, and Verma IM (2007) Intercellular coupling confers robustness against mutations in the SCN circadian clock network. Cell 129:605-616.

Maemura K, Takeda N, and Nagai R (2007) Circadian rhythms in the CNS and peripheral clock disorders: role of the biological clock in cardiovascular diseases. Journal of pharmacological sciences 103:134-138.

Mazuski C, and Herzog ED (2015) Circadian Rhythms: To Sync or Not To Sync. Current Biology 25:R337-R339.

Muraro N, Pirez N, and Ceriani M (2013) The circadian system: plasticity at many levels. Neuroscience 247:280-293.

Nitabach MN, and Taghert PH (2008) Organization of the *Drosophila* circadian control circuit. Current Biology 18:R84-R93.

Peng Y, Stoleru D, Levine JD, Hall JC, and Rosbash M (2003) *Drosophila* free-running rhythms require intercellular communication. PLoS Biol 1:e13.

Pittendrigh CS, and Daan S (1976) A functional analysis of circadian pacemakers in nocturnal rodents. Journal of Comparative Physiology 106:223-252.

Quintero JE, Kuhlman SJ, and McMahon DG (2003) The biological clock nucleus: a multiphasic oscillator network regulated by light. The Journal of neuroscience 23:8070-8076.

Roberts L, Leise TL, Noguchi T, Galschiodt AM, Houl JH, Welsh DK, and Holmes TC (2015) Light Evokes Rapid Circadian Network Oscillator Desynchrony Followed by Gradual Phase Retuning of Synchrony. Current Biology 25:858-867.

Schaap J, Albus H, Tjebbe vanderLeest H, Eilers PH, Détári L, and Meijer JH (2003) Heterogeneity of rhythmic suprachiasmatic nucleus neurons: Implications for circadian waveform and photoperiodic encoding. Proceedings of the National Academy of Sciences 100:15994-15999.

17

Shafer OT, Helfrich-Förster C, Renn SCP, and Taghert PH (2006) Reevaluation of *Drosophila* melanogaster's neuronal circadian pacemakers reveals new neuronal classes. Journal of Comparative Neurology 498:180-193.

Shafer OT, Rosbash M, and Truman JW (2002) Sequential nuclear accumulation of the clock proteins period and timeless in the pacemaker neurons of *Drosophila* melanogaster. The Journal of neuroscience 22:5946-5954.

Sheeba V, Sharma VK, Gu H, Chou YT, O'Dowd DK, Holmes TC (2008) Pigment dispersing factor-dependent and -independent circadian locomotor behavioral rhythms. Journal of Neuroscience 28:217-227.

Sheeba V, Kaneko M, Sharma VK, and Holmes TC (2008) The *Drosophila* circadian pacemaker circuit: Pas de Deux or Tarantella? Critical reviews in biochemistry and molecular biology 43:37-61.

Stanewsky R, Kaneko M, Emery P, Beretta B, Wager-Smith K, Kay SA, Rosbash M, and Hall JC (1998) The cry^b mutation identifies cryptochrome as a circadian photoreceptor in *Drosophila*. Cell 95:681-692.

Stevens RG, and Rea MS (2001) Light in the built environment: potential role of circadian disruption in endocrine disruption and breast cancer. Cancer Causes & Control 12:279-287.

Stoleru D, Nawathean P, de la Paz Fernández M, Menet JS, Ceriani MF, and Rosbash M (2007) The *Drosophila* circadian network is a seasonal timer. Cell 129:207-219.

Tauber E, and Kyriacou BP (2001) Insect photoperiodism and circadian clocks: models and mechanisms. Journal of Biological Rhythms 16:381-390.

Tsumoto K, Kurosawa G, Yoshinaga T, and Aihara K (2011) Modeling light adaptation in circadian clock: Prediction of the response that stabilizes entrainment. PloS one 6:e20880-e20880.

Tyson JJ (2002) Biochemical oscillations. In Computational Cell Biology, pp 230-260, Springer.

Veleri S, Brandes C, Helfrich-Förster C, Hall JC, and Stanewsky R (2003) A self-sustaining, light-entrainable circadian oscillator in the *Drosophila* brain. Current biology 13:1758-1767.

Wang J, Zhang J, Yuan Z, Chen A, and Zhou T (2008) Neurotransmitter-mediated collective rhythms in grouped *Drosophila* circadian clocks. Journal of biological rhythms 23:472-482.

Webb AB, Taylor SR, Thoroughman KA, Doyle III FJ, and Herzog ED (2012) Weakly circadian cells improve resynchrony.

Yamaguchi S, Isejima H, Matsuo T, Okura R, Yagita K, Kobayashi M, and Okamura H (2003) Synchronization of cellular clocks in the suprachiasmatic nucleus. Science 302:1408-1412.

Yamaguchi Y, Suzuki T, Mizoro Y, Kori H, Okada K, Chen Y, Fustin J-M, Yamazaki F, Mizuguchi N, and Zhang J (2013) Mice genetically deficient in vasopressin V1a and V1b receptors are resistant to jet lag. Science 342:85-90.

Yan L, Karatsoreos I, LeSauter J, Welsh D, Kay S, Foley D, and Silver R (2007) Exploring spatiotemporal organization of SCN circuits. In Cold Spring Harbor symposia on quantitative biology, pp 527-541, Cold Spring Harbor Laboratory Press.

Yang Z, and Sehgal A (2001) Role of molecular oscillations in generating behavioral rhythms in *Drosophila*. Neuron 29:453-467.

18

Yao Z, and Shafer O (2014) The *Drosophila* circadian clock is a variably coupled network of multiple peptidergic units. Science 343:1516-1520.

Zhang L, Chung BY, Lear BC, Kilman VL, Liu Y, Mahesh G, Meissner R-A, Hardin PE, and Allada R (2010a) DN1 p circadian neurons coordinate acute light and PDF inputs to produce robust daily behavior in *Drosophila*. Current Biology 20:591-599.

Zhang Y, Liu Y, Bilodeau-Wentworth D, Hardin PE, and Emery P (2010b) Light and temperature control the contribution of specific DN1 neurons to *Drosophila* circadian behavior. Current Biology 20:600-605.

19

Figure Legends

Figure 1. Circadian neurons of cultured whole brain explants exhibit distinct dynamic signatures in constant darkness and when exposed to a phase advancing light pulse. Pseudo-heat maps of individual oscillator *XLG-Per-Luc* expression over time are provided for **A:** 'all cells' (combined across 12 brains per condition) and **B:** each neuronal subgroup. Warmer colors indicate higher amplitude whereas cooler colors indicate lower amplitude of rhythmic *Per* expression. **A (Left):** Cells in DD (n=122) exhibit a wide range of free-running phases with decreasing phase coherence over time. **A (Right):** Cells (n=126) exposed to a 15 min 12.57 W/m^2 white light pulse (LP) at CT 22 on the second day in DD (indicated by dotted black line) generally exhibit a transient reduction in phase coherence and amplitude followed by a phase shift and gradual recovery of phase coherence and amplitude over time. **B (Top)**: L-LNvs (n=25), LNds (n=28), DN1s (n=26), and DN3s (n=22) in DD generally exhibit a loss of phase coherence and amplitude over time to varying degrees with the s-LNvs (n=21) exhibiting the most consistent and robust phase coherence. **B (Bottom)**: S-LNvs (n=24), l-LNvs (n=25), DN1s (n=26), and DN3s (n=22) exposed to the LP exhibit distinct dynamic signatures of transient loss followed by delayed recovery of phase-shifted oscillator synchrony (phase retuning) and amplitude following the LP. Note that the LNds (n=28) appear to exhibit relatively consistent phase coherence and amplitude following the LP, as well as the most rapid phase shift. Raster plots were generated using MATLAB scripts analyzing bioluminescence data reported previously (Roberts et al., 2015).

Figure 2. *Drosophila* circadian neural networks show significant differences in inter- and intra-subgroup dynamics in constant darkness and in response to a phase-advancing light pulse. Circular plots of sine-fit phase estimates using the midpoint of 2-day sliding windows are shown for **A:** individual phases of 'all cells' (combined across all neuronal subgroups from 12 brains) and **B:** phases taken from the mean trace of each neuronal subgroup in **(A, B Top)** constant darkness (DD) and **(A, B Bottom)** following the phase advancing light pulse (LP). The phase angles are shown for s-LNvs (red), l-LNvs (yellow), LNds (orange), DN1s (blue), and DN3s (green). A yellow dotted line divides the general time frames of pre-LP and post-LP exposure. If the resultant vectors end outside of the inner circles (representing the **α** =0.05 threshold for each Rayleigh test; test is not run if there are fewer than 4 rhythmic subgroups), then the phases are significantly concentrated around the mean phase. The null hypothesis is that the phases are uniformly distributed. In **2B**, the mean phases for neuronal subgroups were excluded at certain time points if the subgroup: (1) did not have any reliably rhythmic cells at that time point or (2) did not have sufficient phase coherence to provide a reliable mean phase estimate. **C:** Snapshots of selected time points from **Supp. Movie 1** showing changes in single oscillator phase and amplitude over time in DD (left) and in response to the LP (right). The LP is represented by a yellow highlight on day two. The disks representing each of the subgroups are colored the same as previous figures. The angle of the disks around the circle represents phase and the distance of the disks from the center represents amplitude. Phase and amplitude were

estimated using 2-dimensional embedding applied to wavelet detrended traces for each individual oscillator. Circular phase plots were generated using MATLAB scripts. See 'Experimental Procedures' for details.

Figure 3. Quantification of neuron subgroups' dynamics in constant darkness reveals distinct differences in phases, periods, and degrees of phase dispersion over time. Phases of individual oscillators categorized by neuronal subgroup are shown in circular plots based on sine-fit phase estimates using the midpoint of 2-day sliding windows. To compare relative phase shifts over time, phases were normalized such that overall mean phase for Day 1 for 'all cells' is circadian time 0 (CT 0). Neuronal subgroups in DD reveal a wide range of phases and periods and generally exhibit gradual phase dispersion over time; with the notable exception of the s-LNvs. If the resultant vectors end outside the inner circles, then the phase distribution significantly differs from the uniform distribution. The absence of plots for certain time points indicates that rhythmicity for all oscillators was too damped for reliable sine-fit measures.

Figure 4. Neuronal subgroups exposed to a phase-advancing light pulse exhibit distinct dynamics of loss and recovery of phase-shifted synchronous oscillations. Circular phase plots reveal distinct neuronal subgroups' dynamics of phase response to a light pulse (the yellow dotted line divides the general time frames of pre-LP and post-LP exposure). Neuronal subgroups generally exhibit significant phase dispersion following exposure to the LP, with the exception of the LNds and DN3s. Relative to corresponding subgroups in DD, neuronal subgroups also generally exhibit significantly greater phase coherence and a shift in mean phase 3-4 days after the light pulse. The inner circles represent the α =0.05 threshold for each Rayleigh test, with the null hypothesis that phases are uniformly distributed.

Figure 5. Mathematical modeling of circadian network dynamics indicates importance of complementary coupling of strong and weak oscillators in synchronization and adaptation. The general dynamic signatures of oscillator synchrony and phase retuning by light are modeled using three oscillator groups coupled by complementary activating and repressing signals. **A:** Three oscillator groups (60 oscillators total) are simulated in either constant darkness (**A, Left**) or in response to a phase advancing light pulse (**A, right**), using a modified version of the Goodwin model (Tyson, 2002). Traces of the *Z* variable are shown here. Rate parameters are set to generate damped circadian oscillations. Group 1 (10 oscillators) is light responsive and sends a signal that increases transcription rate. Group 2 (10 oscillators) is light responsive, has a shorter period, and sends a signal that decreases transcription rate. Group 3 (40 oscillators, but only 10 representative oscillators shown in figures for clarity) is not directly light responsive, more strongly damped, and send a signal that decreases transcription rate. **B:** Mean traces of the Z variable from each of the three groups of oscillators show that group 2 oscillators exhibit an increase in amplitude following the LP and are the first group to exhibit a phase advance. **C:** As observed with bioluminescence data, the simulated oscillators exposed to a phase advancing light pulse (red trace) exhibit a mean decrease in order parameter R, followed by a delayed increase in R relative to oscillators in DD (black trace). R varies between 0 and 1 with higher values

21

1
2
3
4
5
6
7
8
9
10
11
12
13
14
15
16
17
18
19
20
21
22
23
24
25
26
27
28
29
30
31
32
33
34
35
36
37
38
39
40
41
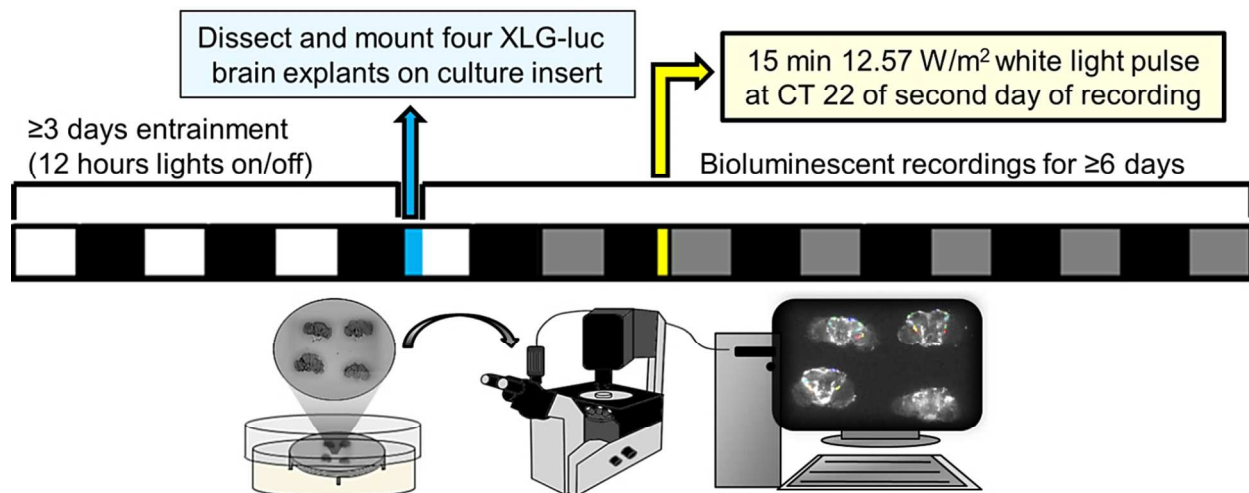42
43
44
45
46
47
48
49
50
51
52
53
54
55
56
57
58
59
60

indicating similarity in phase, period, and waveform. **D:** Phase response curves of simulated systems, with all oscillators having only excitatory signals (activating only), only inhibitor signals (repressing only), or a complementary system with a mix of both signaling types. **E:** Simulations in constant darkness show that the complementary system shows an intermediate period length relative to activating only and repressing only systems. Simulations were generated using custom MATLAB scripts. See Materials and Methods for details.

1
2
3
4
5
6
7
8
9
10
11
12
13
14
15
16
17
18
19
20
21
22
23
24
25
26
27
28
29
30
31
32
33
34
35
36
37
38
39
40
41
42
43
44
45
46
47
48
49
50
51
52
53
54
55
56
57
58
59
60

Functional Contributions of Strong and Weak Cellular Oscillators to Synchrony and

Light-Shifted Phase Dynamics

Logan Roberts, Tanya L. Leise, David K. Welsh, and Todd C. Holmes

Supplementary Online Material

Figure S1. General schematic of the experimental setup for bioluminescence recordings. Adult, male *XLG-Per-Luc* flies are entrained to a standard 12 hr:12 hr LD schedule for ≥3 days (white and black squares represent 12 hour light and dark periods, respectively). Four adult male flies are then dissected and mounted on a culture membrane insert in a 35 mm dish containing 1.2 ml of culture medium. 1 mM luciferin is added to the culture medium 30 minutes prior to recording. The cultured brains are then placed on the stage of an Olympus IX71 inverted microscope set in a dark room. Light from the samples is collected by a 4x objective and transmitted directly to a cooled charge-coupled device (CCD) camera mounted on the microscope's bottom port. *XLG-Per-Luc* bioluminescence images are collected by a computer at 30 minute intervals and analyzed with the software MetaMorph and custom MATLAB scripts. For baseline measurements, bioluminescence recordings were obtained for whole brain explants maintained in constant darkness. These recordings were compared to brain explants exposed to a 12.57 W/m2 (2,000 lux), 15 minute light pulse at CT 22 on the second day of imaging. Only experiments which had all four brains still healthy, intact, free of contamination, adherent to the insert membrane, and exhibiting bioluminescence for ≥ 6 days were analyzed. See "Materials and Methods" for specific details on setup.
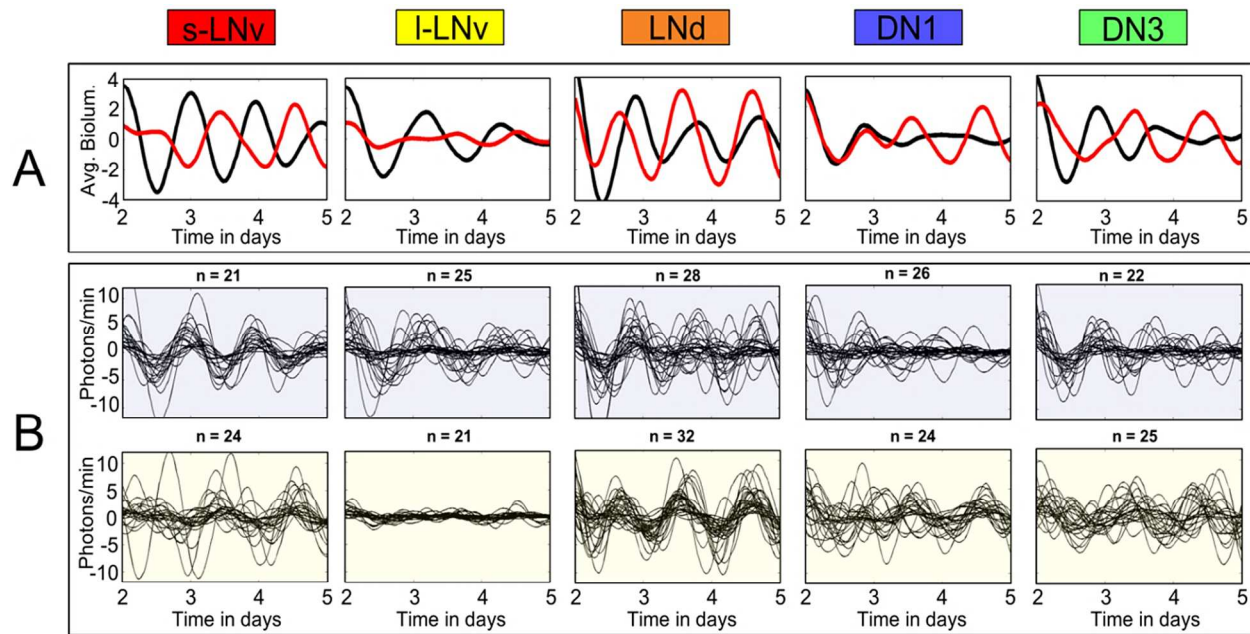
Figure S2. Distinct differences in phase, synchrony and amplitude observed between strong versus weak oscillators in DD and in response to a phase advancing light pulse. *XLG-Per-Luc* bioluminescence time-series measurements show the dynamics of neuronal oscillators either maintained in constant darkness ("DD cells") or after exposure to a 15 minute light pulse at CT 22 on the second day in DD ("LP cells") as previously reported (Roberts et al., 2015). The time frames were narrowed to cover day 2 to day 5 of the recording in order to more clearly highlight the dynamic changes in activity during this critical window. **A:** Comparing mean bioluminescence traces confirms that LP cells (red line) exhibit a transient loss then recovery of phase shifted synchrony in response to the light pulse relative to DD cells (black line). Note that the LNds also exhibit the most immediate, high fidelity phase shift of two hours following the LP. **B**: Wavelet-detrended time series are shown comparing neuronal subgroup dynamics in either DD (top panel) or LP (bottom panel) conditions. The number of neuronal oscillators analyzed for each condition and subgroup are shown above each panel.

1
2
3
4
5
6
7
8
9
10
11
12
13
14
15
16
17
18
19
20
21
22
23
24
25
26
27
28
29
30
31
32
33
34
35
36
37
38
39
40
41
42
43
44
45
46
47
48
49
50
51
52
53
54
55
56
57
58
59
60
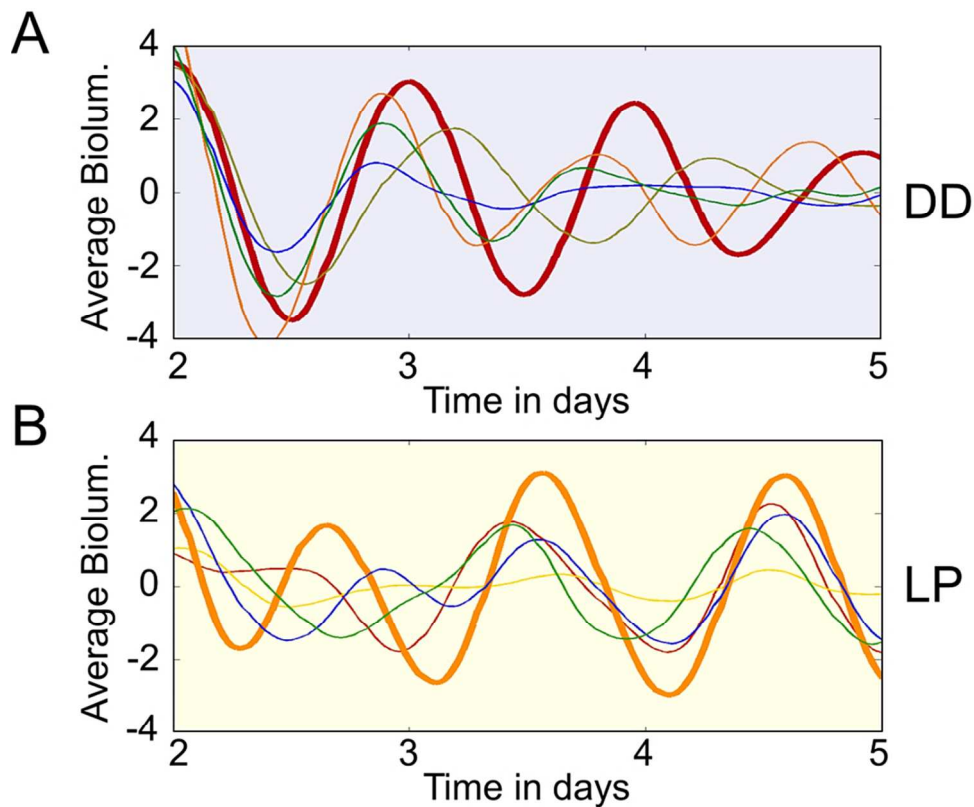
Figure S3. Alignment of inter-subgroup dynamics indicates role of strong oscillators in both DD and LP conditions. Mean bioluminescence traces are provided for the sLNvs (red), l-LNvs (yellow), LNds (orange), DN1s (blue) and DN3s (green). **A:** Subgroups in DD exhibit a gradual decrease in rhythmicity and inter-subgroup synchrony over time. Note that the s-LNv trace is slightly thicker to highlight this subgroup having the most consistently high amplitude oscillations in DD relative to other subgroups. **B:** After exposure to a phase-advancing light pulse, most subgroups show suppressed amplitudes and scrambled phases. The LNds are represented with a thicker trace to highlight that these oscillators exhibit an increase in amplitude and synchrony following exposure to the LP.
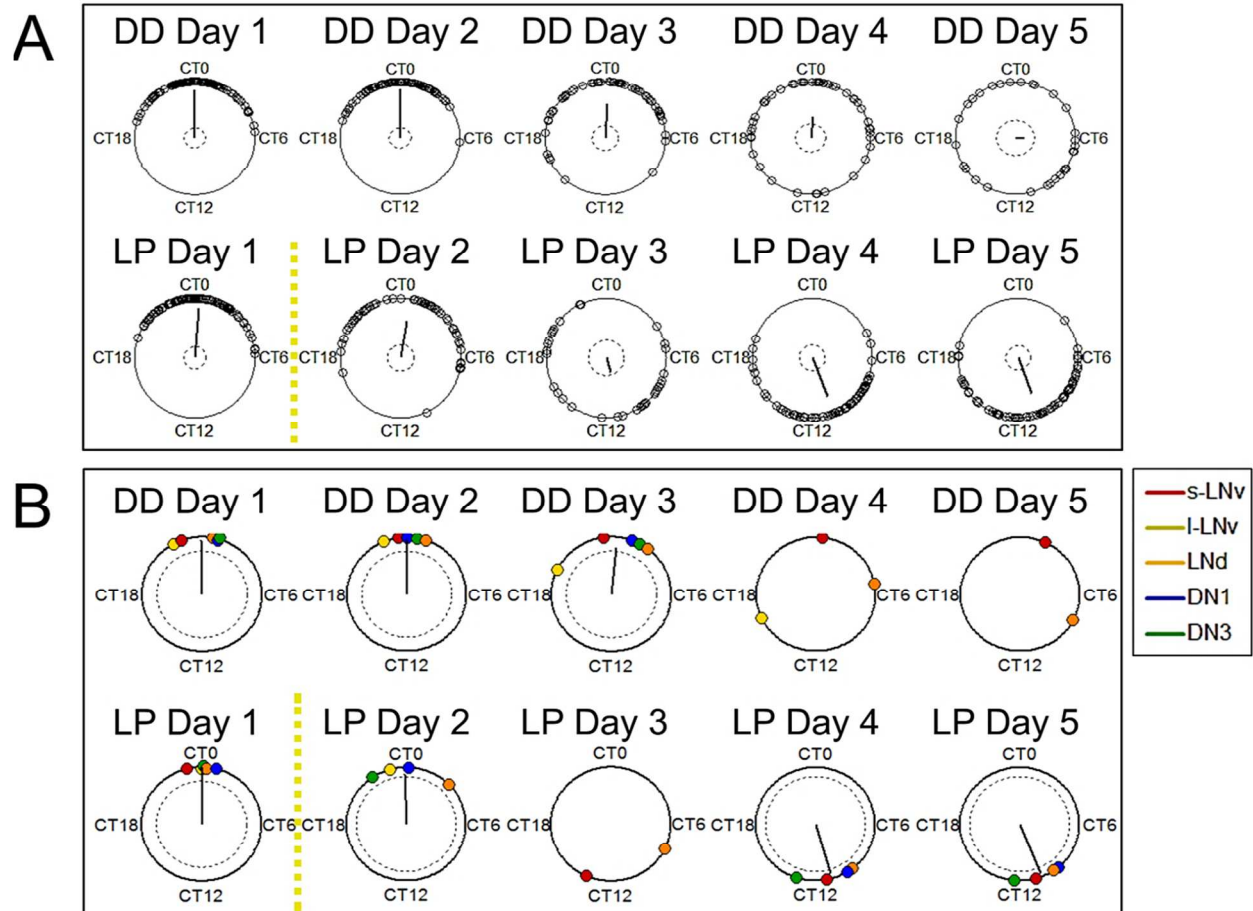
Figure S4. Nonlinear embedded phase estimates show the same trends in phase coherence and mean phase over time in DD and after LP as observed with sine-fit estimates. Circular phase plots for 'all cells' (combined across all neuronal subgroups) in **A:** DD and **B:** after a light pulse reveal the same patterns in phase coherence and phase shift as observed for sine-fit estimates in Fig. 2A. The similarity in trends using both methods confirms the reliability and consistency of observations made using the sine-fit estimates in combination with discrete wavelet transform. Custom MATLAB scripts were used to generate nonlinear embedded phase plots. See Fig. 2A for description of phase plots.
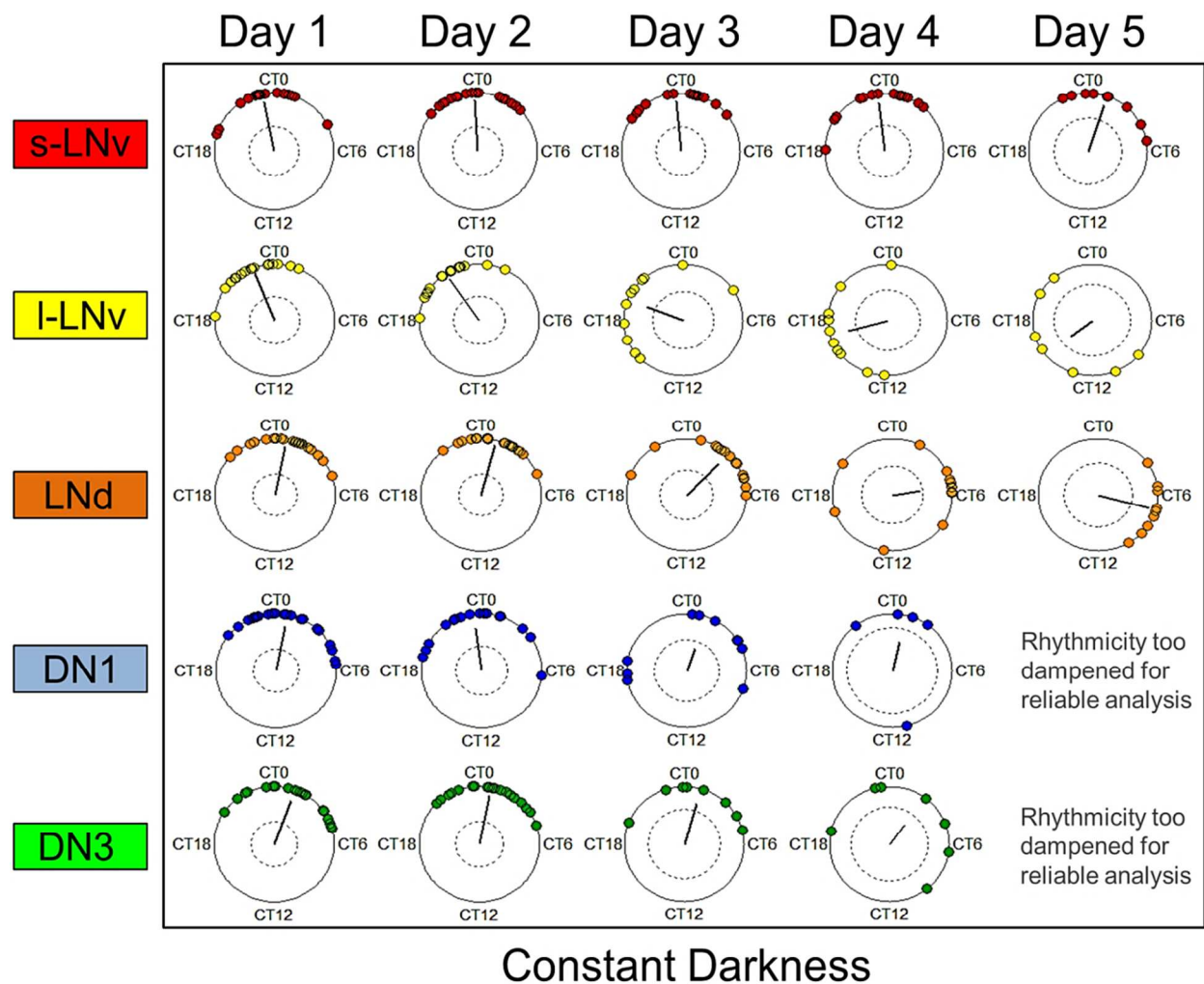
Figure S5. Nonlinear embedded estimates of neuronal subgroups maintained in DD show general phase dispersion and phase drift over time in DD. Embedded phase plots for neuron subgroups maintained in DD confirm the same trends of phase dispersion as observed using sine-fit estimates in Fig. 3. See Fig. 3 for description of circular phase plots for neurons in DD.
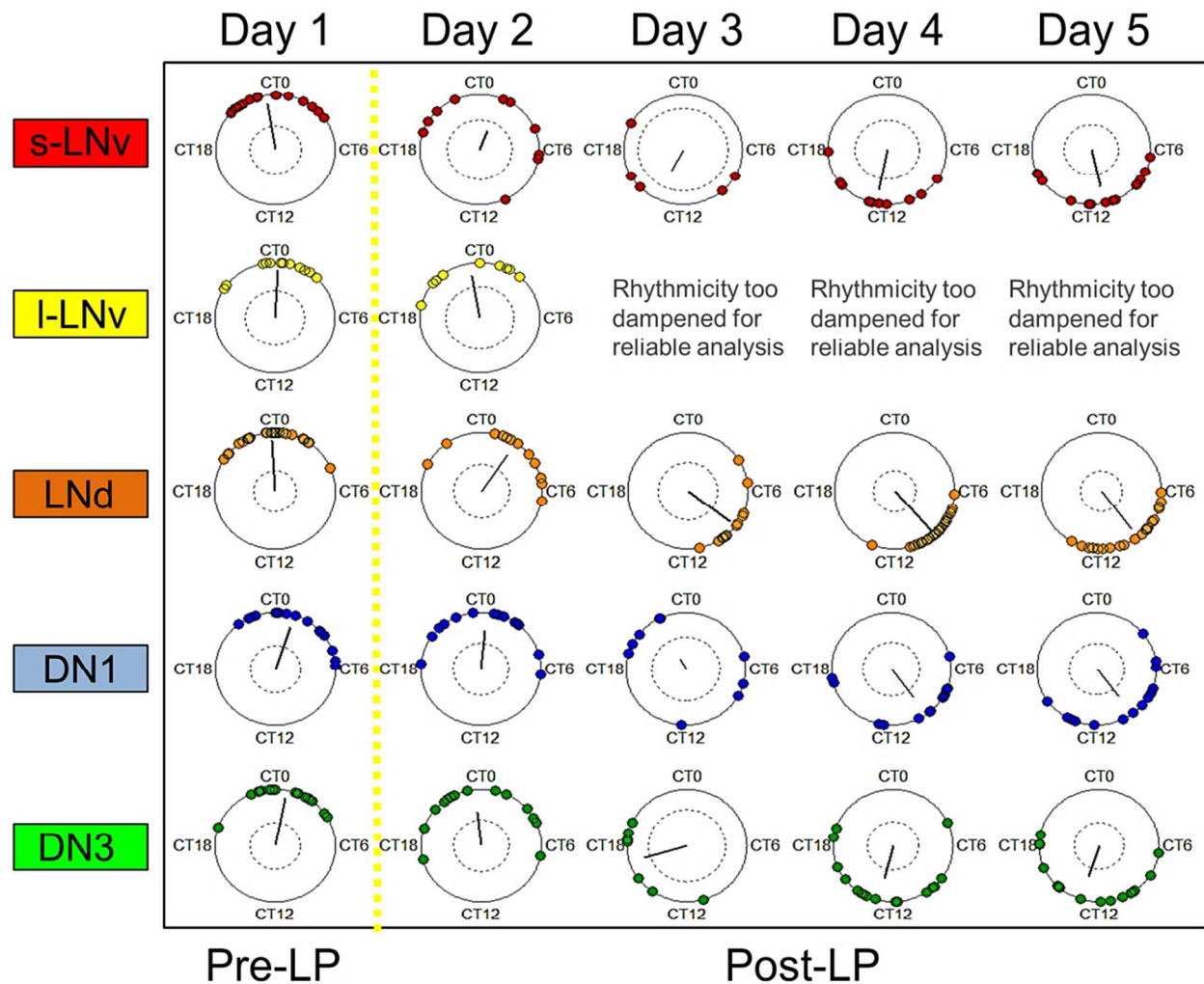
Figure S6. Nonlinear embedded phase estimates of neuronal subgroups exposed to a light pulse generally show transient phase dispersion followed by delayed increase in phase coherence. Circular phase plots for neurons exposed to a light pulse show the same general patterns of transient phase dispersion followed by delayed phase increase and phase shift, using the nonlinear embedded method (as seen here) and the sine-fit method (seen in Fig. 4). See Fig. 4 for details regarding circular phase plots for neurons exposed to a LP.

Statistics on Phase Sine vs Embed Phase Estimates (Circ. correlation for phase)		
Condition + Day	Rho	p-value
DD day 1	0.98	3.60E-12
LP day 1	0.98	3.60E-12
DD day 2	0.94	3.20E-10
LP day 2	0.93	1.80E-09
DD day 3	0.96	3.40E-10
LP day 3	0.97	3.10E-09
DD day 4	0.96	6.40E-08
LP day 4	0.96	1.90E-07
DD day 5	0.96	9.50E-06
LP day 5	0.98	7.90E-11

Table S1. Nonlinear embedded phase analysis validates sine-fit estimates of phase. Custom MATLAB scripts were used to calculate the correlation coefficients (rho) and p-values between nonlinear embedded and sine-fit phase estimates across all neuronal subgroups for all time points and conditions. The p-value is based on the null hypothesis that there is no correlation in phase estimates between these two methods. The strong positive, linear correlation (indicated by high rho values) and low p-values confirm that sine-fit estimates of phase using two-day sliding windows are accurate. The same neurons were analyzed using both methods for corresponding time points, subgroups, and conditions.

Supplemental Movie 1. Please see online for animations of individual oscillator dynamics in DD and in response to a phase advancing light pulse show the complexity of the network phase ensemble. The animations show changes in the phase and amplitude of XLG-Per-Luc bioluminescence activity for individual oscillators from all neuronal subgroups in either DD (Left, n=122) or in response to a phase advancing light pulse (Right, n=126). The timing of the LP is indicated by a yellow highlight around the circle. The angle of the disks represents phase and drift of the disks towards the center of the circle and the size of the disks indicates reduction in amplitude. The disks are colored according to neuronal subgroup for the s-LNvs (red), l-LNvs (yellow), LNds (orange), DN1s (blue) and DN3s (green). Animations were generated using custom MATLAB scripts. See Materials and Methods for details.

Supplemental Movie 2. Animations of individual subgroup dynamics show that the activities of neuronal subgroups are transiently scrambled before a phase advance by a light pulse. Changes in average phase and amplitude over time are animated for circadian neuronal subgroups. Note that the LNds appear to lead the phase advance while the phases and amplitudes of the other neuronal subgroups are transiently scrambled following the light pulse. The same color scheme, nonlinear dynamics method, and data sets were used as seen in Movie S1.

Supplemental Movie 3. Animations of averaged network kinetics show a transient reduction in amplitude by the light pulse followed by delayed recovery of phase-shifted amplitude over time. The average activity of whole network (i.e. averaged from all neuronal subgroups) dynamics in either DD (Left) or in response to the phase advancing light pulse (Right) are represented by black disks. See Movie S1 for details regarding measures and representations of phase and amplitude.

1
2
3
4
5
6
7
8
9
10
11
12
13
14
15
16
17
18
19
20
21
22
23
24
25
26
27
28
29
30
31
32
33
34
35
36
37
38
39
40
41
42
43
44
45
46
47
48
49
50
51
52
53
54
55
56
57
58
59
60

Functional Contributions of Strong and Weak Cellular Oscillators to

Synchrony and Light-Shifted Phase Dynamics

Logan Roberts, Tanya L. Leise, David K. Welsh, and Todd C. Holmes

Supplementary Online Material: Mathematical Modeling

We developed a simple mathematical model to explore the qualitative dynamics of a network composed of different oscillator types, based on current knowledge of the *Drosophila* circadian network. The modeling aim here is to observe the key general features of the various oscillator types and demonstrate how a mix of activating and repressing coupling mechanisms in a system with different oscillator types may support circadian properties like amplitude, synchrony, period length, and entrainment. We do not propose to employ the model to provide evidence for how the circadian circuit responds to a phase shifting light pulse in such a fashion but instead suggest why it appears to respond in such a way (i.e. potential consequences of the heterogeneous network). Previous studies have shown that alterations in coupling between heterogeneous oscillator types can result in different emergent periods and phases (Tokuda et al., 2005).

The *Drosophila* clock consists of clusters of clock neurons with distinct circadian properties, with both excitatory and inhibitory intercellular signals playing roles in determining the system's overall properties, such as period length (Dissel et al., 2014). Rather than one cluster acting as a master pacemaker controlling the others, the different clusters each play important and functionally distinct roles (Yao and Shafer, 2014). Multiple coupling signals are released from and perceived by various *Drosophila* clock neurons, including PDF, which stimulates cAMP near dawn, and glutamate, which inhibits cAMP around dusk, thereby generating differentially timed synchronizing signals to promote robust oscillations (Collins et al., 2014). Inspired by these general principles underlying the *Drosophila* circadian clock, we built a model system involving three groups of oscillators with distinct types of signaling, light responses, and degrees of dampening. However, the groups in this model are not intended to specifically represent particular clock neuron clusters, and the coupling mechanisms in the model are not meant to represent specific neurotransmitters. The main premise is to demonstrate through a relatively simple model how different dynamic signatures could be generated through a heterogeneous circadian system and what the advantages of such a system might be.

Each oscillator is simulated using a modified version of the Goodwin model (Bliss et al., 1982; Tyson, 2002):

$$\frac{dX}{dt} = \frac{a(1 + k_{act} - k_{rep})}{Z + 1} - bX \quad (1)$$

$$\frac{dY}{dt} = bX - bY \quad (2)$$

$$\frac{dZ}{dt} = bY - \frac{cZ}{Z + 1} \quad (3)$$

Various versions of Goodwin-type models have been employed to study the circadian system (Ruoff et al., 2001; Cheng et al., 2009; Saithong et al., 2010; Komin et al., 2011; Leise et al., 2013; Gu et al., 2014; Kidd et al., 2015; Gu et al., 2015). The parameters for our system (see Table 1) are set so that uncoupled oscillations dampen over time toward the steady state values,

$$X_{ss} = Y_{ss} = \frac{a}{b(1+a/c)} \text{ and } Z_{ss} = \frac{a}{c}.$$

Although the individual oscillators are damped, the coupled system described below generates sustained oscillations for $\beta > 0.03$ under constant conditions, and also entrains to light-dark cycles (see Figure 1).

	s	a	b	c	β
Group 1	0.98 ± 0.005	$(9s\text{-}1)c$	$0.149\text{-}0.1535$	$81bs^2$	0.035 ± 0.007
Group 2	0.98 ± 0.005	$(9s\text{-}1)c$	$0.1525\text{-}0.157$	$81bs^2$	0.035 ± 0.007
Group 3	0.88 ± 0.005	$(9s\text{-}1)c$	$0.149\text{-}0.157$	$81bs^2$	0.175 ± 0.035

Table M1. Parameter values for modified Goodwin model. The model generates self-sustained oscillations in individual oscillators if $s>1$ and damped oscillations if $s<1$ (with smaller s leading to faster damping). To create heterogeneity in the oscillator groups, values of s and β are normally distributed random numbers with the indicated mean and standard deviation, while values for b are evenly distributed in the indicated range for each group (not random). Parameters a and c are fixed functions of s and b; see (Tyson, 2002) for the derivation of these relations via a linear stability analysis. Group 3 needs a stronger coupling signal to maintain rhythmicity, due to its low value of s (strongly damped).

To explore the dynamic interactions of damped oscillators with different properties, we created a network of 60 modified Goodwin oscillators organized into 3 groups. "Group 1" oscillators (10 total, #1-10) are directly light responsive, weakly damped, and send an activating coupling signal that effectively increases the transcription rate a of all oscillators when the Group 1 oscillators have X levels above the theoretical steady state value X_{ss}. "Group 2" oscillators (10 total, #11-20) are more strongly light responsive, weakly damped, and transmit a repressing coupling signal that effectively decreases the transcription rate a of all oscillators when the Group 2 oscillators have Z levels above the steady state value Z_{ss}. These coupling functions were chosen to appropriately time the signals to promote synchronization. In both cases, higher amplitude oscillations lead to stronger coupling. "Group 3" oscillators (40 total, #21-60) are not directly light responsive, strongly damped, and send a repressing coupling signal like that of Group 2.

Light response is achieved through increasing the degradation rate parameter c in equation (3). Both LD entrainment and response to light pulses can be effectively modeled through this mechanism. For example, a light pulse simulated by increasing c by 8% for Group 1 oscillators and by 16% for Group 2 oscillators for 4 hours starting 3 hours before the peak in mean X results in a large phase advance for the coupled system. LD entrainment can be simulated by increasing c by 0.4% for Group 1 oscillators and by 0.8% for Group 2 oscillators for the first 10h of each 24h day. In all simulations, the system is entrained to LD for 500 days, released into DD for 2 weeks, then the light pulse is administered.
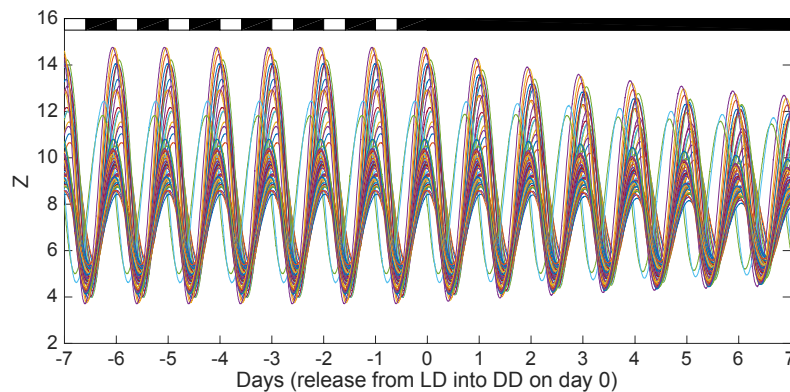
Figure M1. Oscillations of the 60-oscillator system under LD entrainment, showing release into DD. Mixed coupling, with parameters as shown in Table 1.

Coupling is achieved through modifying the transcription rate parameter a in equation (1). Two complementary types are used for the modeling: k_{act} increases transcriptional activation while k_{rep} represses transcription (see Figure 2):

$$k_{act} = \frac{\beta}{10} \sum_{n=1}^{10} \frac{\max(X_n - X_{ss}, 0)}{X_{ss} + \max(X_n - X_{ss}, 0)},$$

$$k_{rep} = \frac{\beta}{50} \sum_{n=11}^{60} \frac{\max(Z_n - Z_{ss}, 0)}{Z_{ss} + \max(Z_n - Z_{ss}, 0)}.$$

All oscillators receive both types of coupling signals, but each group sends a single type of coupling signal. Note that in the alternate simulations where only one type of coupling is used, then all three groups send the indicated type of signal (activating or repressing). For the case of activating-only coupling signals, the coupling functions are

$$k_{act} = \frac{\beta}{10} \sum_{n=1}^{10} \frac{\max(X_n - X_{ss}, 0)}{X_{ss} + \max(X_n - X_{ss}, 0)} + \frac{\beta}{50} \sum_{n=11}^{60} \frac{\max(X_n - X_{ss}, 0)}{X_{ss} + \max(X_n - X_{ss}, 0)}, \quad k_{rep} = 0,$$

while for the case of repressing-only coupling signals, the coupling functions are

$$k_{act} = 0 \,, \;\; k_{rep} = \frac{\beta}{20} \sum_{n=1}^{10} \frac{\max(Z_n - Z_{ss}, 0)}{Z_{ss} + \max(Z_n - Z_{ss}, 0)} + \frac{\beta}{50} \sum_{n=11}^{60} \frac{\max(Z_n - Z_{ss}, 0)}{Z_{ss} + \max(Z_n - Z_{ss}, 0)} \,.$$
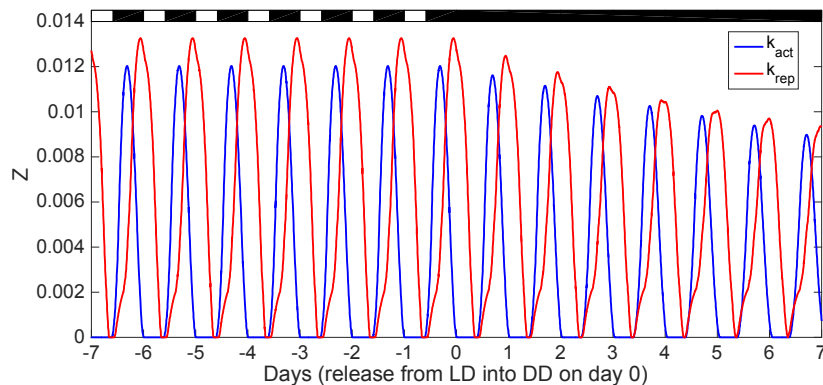

Figure M2. Coupling functions k_{act} and k_{rep} under LD entrainment followed by DD. Mixed coupling, with parameters as shown in Table 1.
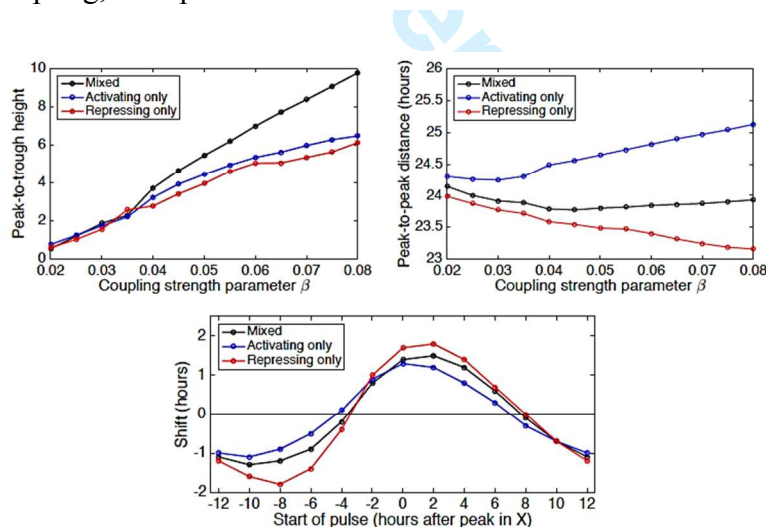

Figure M3. Short-term characteristics of system after release from LD into DD. *Upper left*: Peak-to-trough height of the mean Z waveform 2 weeks after release from LD entrainment to DD. *Upper right*: Distance between consecutive peaks of the mean Z waveform 2 weeks after release from LD entrainment to DD. *Lower*: Phase response curve for 30-minute light pulse for $\beta=0.035$. Simulations used the parameter values in Table 1 (except β as indicated in the graphs), with three different types of coupling. As β increases, the mixed coupling results in a more

slowly changing cycle length and higher amplitude compared to the activating-only and repressing-only cases.
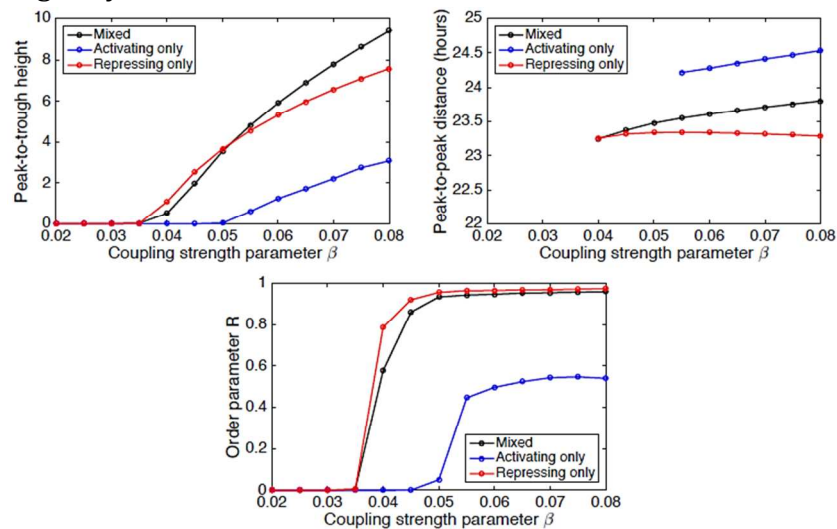
Figure M4. Long-term characteristics of the system under DD. *Upper left*: Amplitude of the mean Z waveform under long-term DD, with positive amplitude indicating self-sustained oscillations of the coupled system. *Upper right*: Period under long-term DD for cases with self-sustained oscillations. *Lower*: Order parameter R calculated using Z under long-term DD. Simulations used the parameter values in Table 1 (except β as indicated in the graphs) for 1000 days, with three different types of coupling. As β increases, the mixed coupling results in a more moderate cycle length and higher amplitude compared to the activating-only and repressing-only cases. β=0.035 is the threshold for the system to exhibit stable oscillations over long term for mixed and repressing-only cases. The presence of repressing coupling supports stable oscillations over the long run for the system (after transients settle out, which usually took 200-300 days).

To quantify changes in synchrony over time, we use the order parameter R, defined as in (Gonze et al., 2005) for a system of N oscillators with state variable X:

$$R = \frac{\langle X^2 \rangle - \langle X \rangle^2}{\frac{1}{N}\sum_{k=1}^{N}\left(\langle X_k^2 \rangle - \langle X_k \rangle^2\right)},$$

where angle brackets denote time average and $X = \frac{1}{N}\sum_{k=1}^{N} X_k$. If the phase, period and waveform of all N cells are in perfect synchrony then R=1, while a uniform distribution of phases would lead to R=0.

1
2
3
4
5
6
7
8
9
10
11
12
13
14
15
16
17
18
19
20
21
22
23
24
25
26
27
28
29
30
31
32
33
34
35
36
37
38
39
40
41
42
43
44
45
46
47
48
49
50
51
52
53
54
55
56
57
58
59
60

Figures M5-7 below show the results of a strong advancing light pulse for the 60-oscillator system with 10 in group 1, 10 in group 2, and 40 in group 3. In all light pulse simulations, the system is first entrained to a light-dark cycle for 500 days as described above, then released to constant conditions for two weeks before the 4-hour light pulse is administered, with the start of the light pulse 3 hours before the peak in mean X. For comparison, Figure M8 shows the results of a strong delaying light pulse for the same system, using a 4-hour light pulse starting 8 hours before the peak in mean X.

Shifts are determined by comparing the peak times of the mean Z trace for unpulsed versus light-pulsed conditions on the 6th day following the light pulse, chosen because the experiments only ran that length of time.
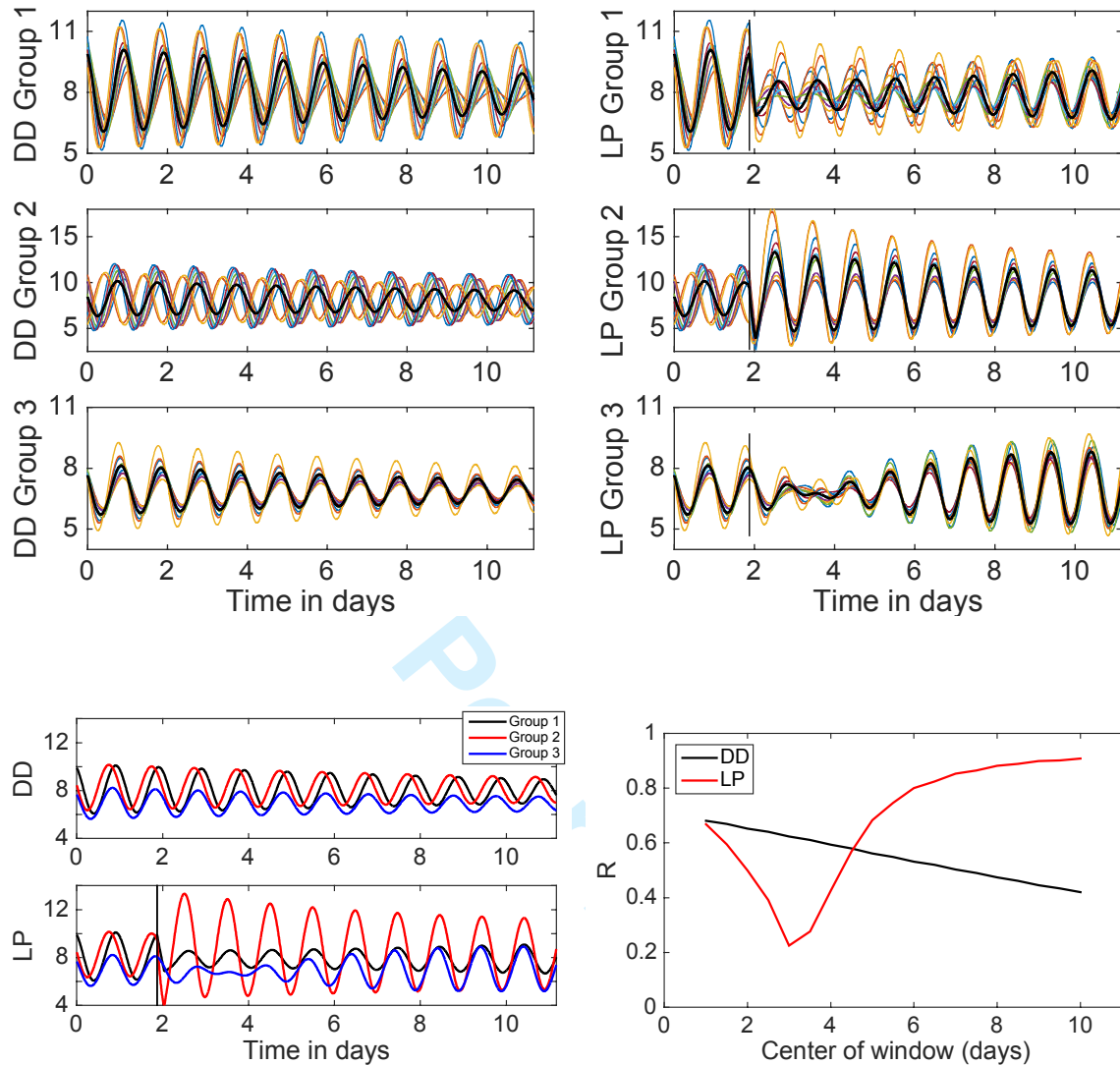
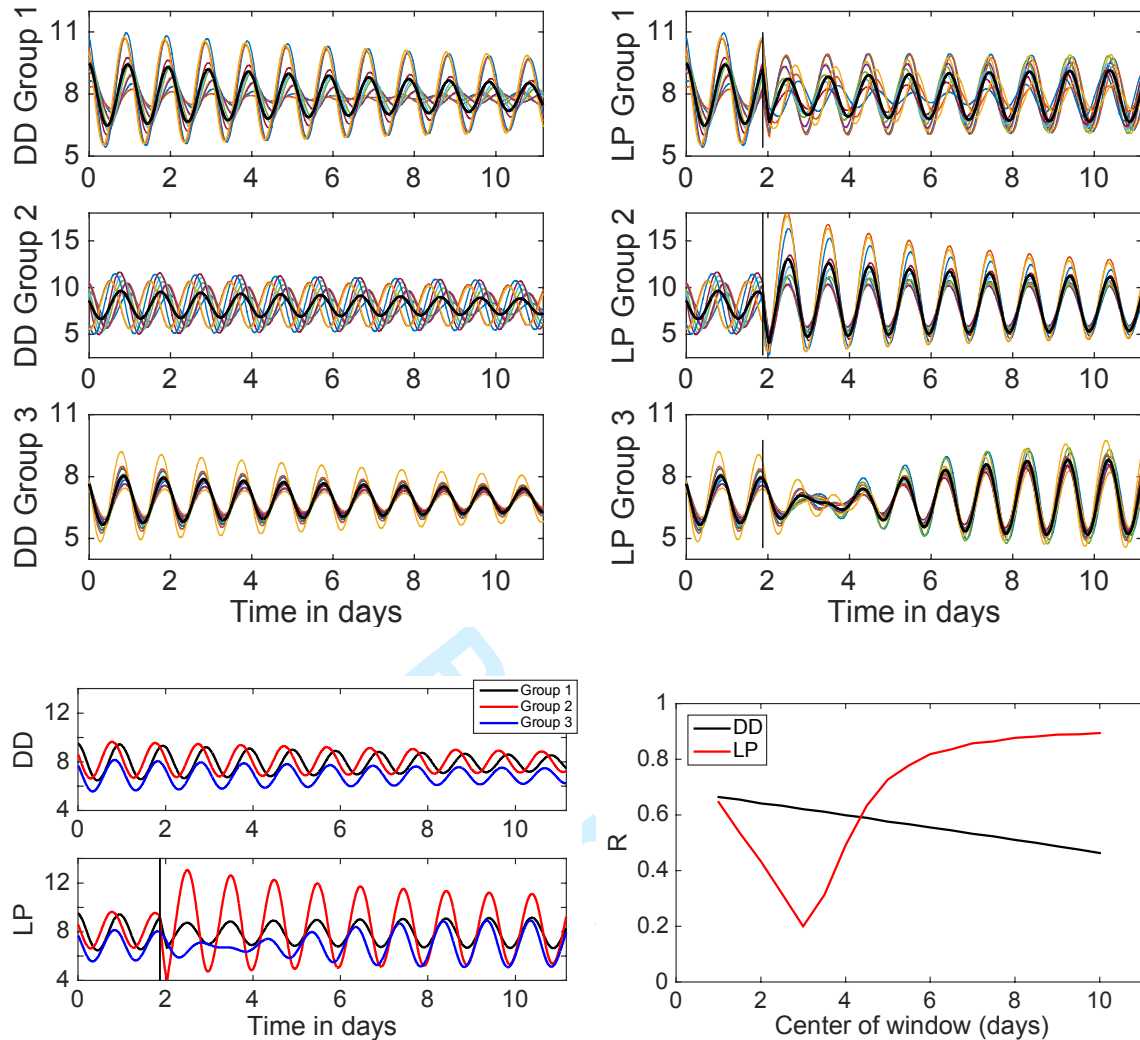**Figure M5. Large phase advance of 8.6h for 60-oscillator system with mixed coupling and β =0.035.** *Top*: traces of the 10 group 1 oscillators, traces of the 10 group 2 oscillators, and traces of 10 representative group 3 oscillators under constant conditions (DD) or with a 4h light pulse applied 3h before the peak in mean X (LP). A vertical line marks the time of start of the light pulse. *Lower left*: mean traces for each group. *Lower right*: order parameter R for 2-day windows, calculated using Z.
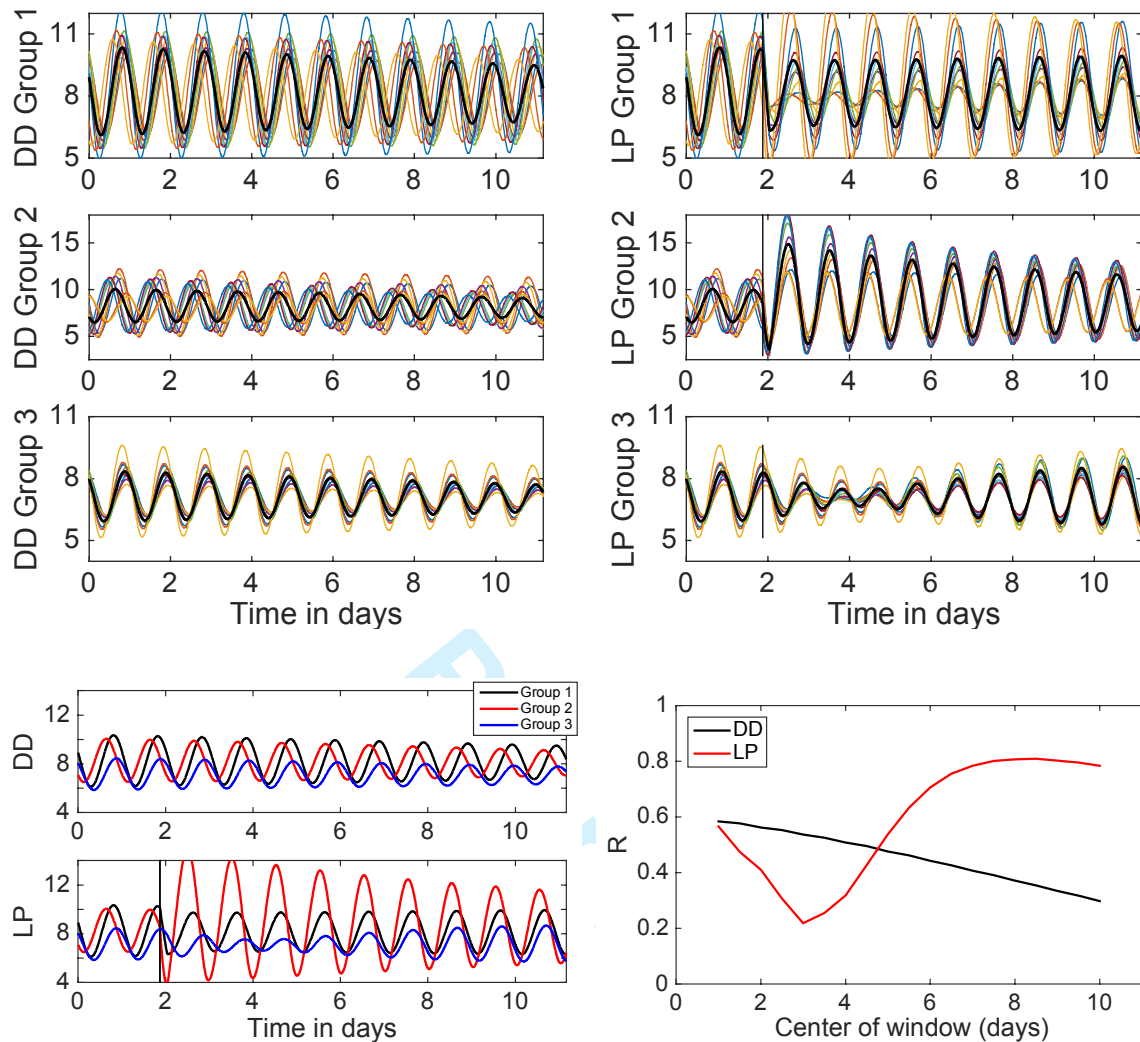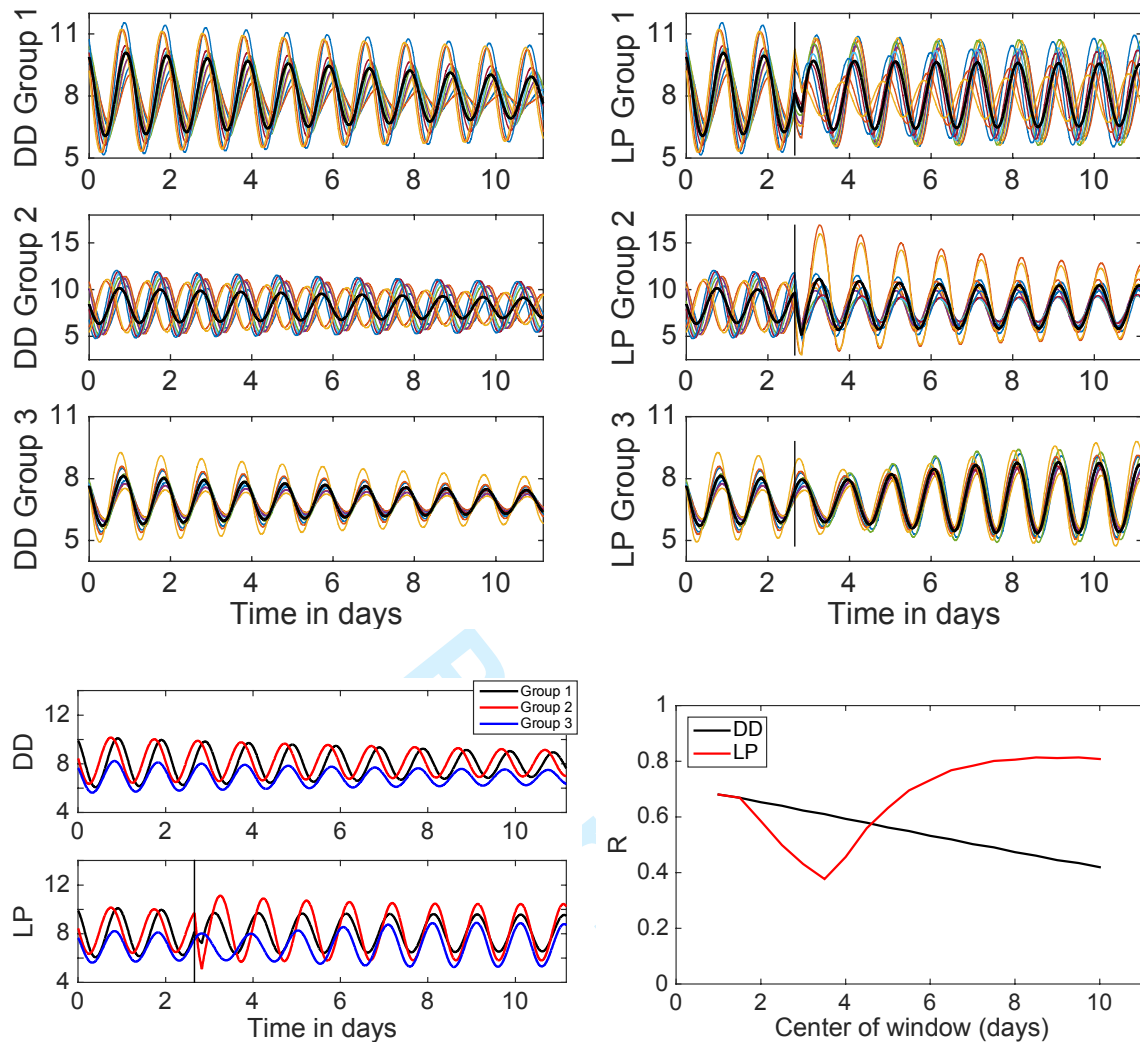
Figure M6. Large phase advance of 6.6h for 60-oscillator system with activating-only coupling and *β* =0.035. *Top*: traces of the 10 group 1 oscillators, traces of the 10 group 2 oscillators, and traces of 10 representative group 3 oscillators under constant conditions (DD) or with a 4h light pulse applied 3h before the peak in mean *X* (LP). A vertical line marks the time of start of the light pulse. *Lower left*: mean traces for each group. *Lower right*: order parameter *R* for 2-day windows, calculated using *Z*.

Figure M7. Large phase advance of 8.4h for 60-oscillator system with repressing-only coupling and β =0.035. *Top*: traces of the 10 group 1 oscillators, traces of the 10 group 2 oscillators, and traces of 10 representative group 3 oscillators under constant conditions (DD) or with a 4h light pulse applied 3h before the peak in mean X (LP). A vertical line marks the time of start of the light pulse. *Lower left*: mean traces for each group. *Lower right*: order parameter R for 2-day windows, calculated using Z.

Figure M8. Large phase delay of 8.1h for 60-oscillator system with mixed coupling and β =0.035. *Top*: traces of the 10 group 1 oscillators, traces of the 10 group 2 oscillators, and traces of 10 representative group 3 oscillators under constant conditions (DD) or with a 4-hour light pulse applied 8 hours before the peak in mean X (LP). A vertical line marks the time of start of the light pulse. *Lower left*: mean traces for each group. *Lower right*: order parameter R for 2-day windows, calculated using Z.

To further assess the roles of each group and type of coupling, the figures below examine different scenarios through phase response curves to half-hour light pulses and through the order parameter R for the stronger 4-hour light pulse (applied 3 hours before peak in mean X). The cases of mixed coupling and repressing-only coupling lead to stronger synchronization in DD as the coupling strength β increases. In the case of activating-only coupling, increasing the coupling strength has a more limited effect. For all three cases and values of β near 0.035, the advancing light pulse causes a transient dip in R followed by an overshoot.

Left: Phase response curve for a 30-minute light pulse. Negative shifts indicate delays, while positive shifts correspond to advances.
Right: Order parameter R, calculated using Z, in DD versus following a 4h light pulse that begins 3 hours before peak in X, which results in a large phase advance.
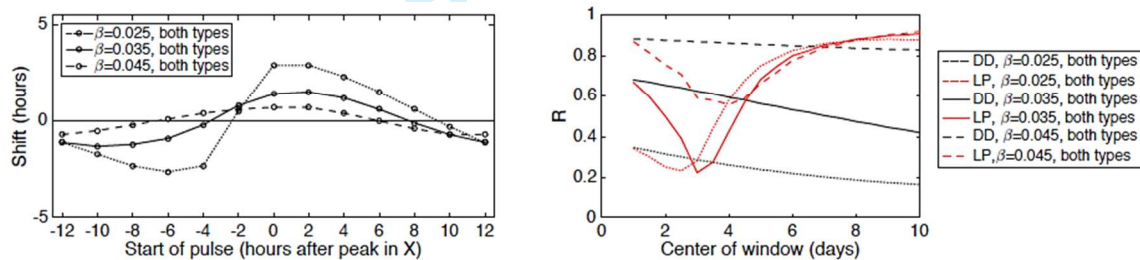
Figure M9. Both types of coupling signals are present (the base model).
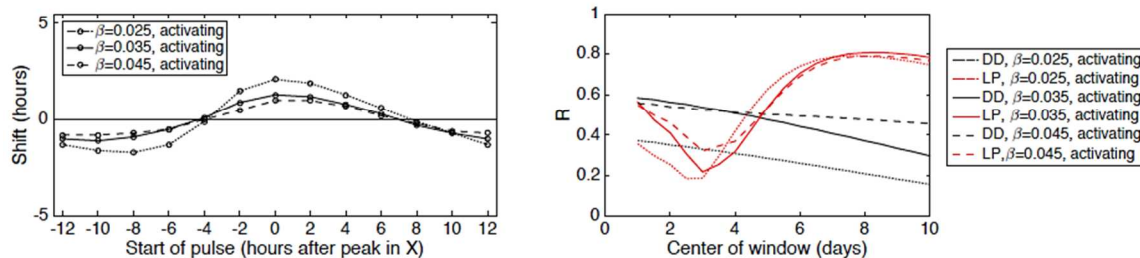
Figure M10. Coupling from all three groups is activating.
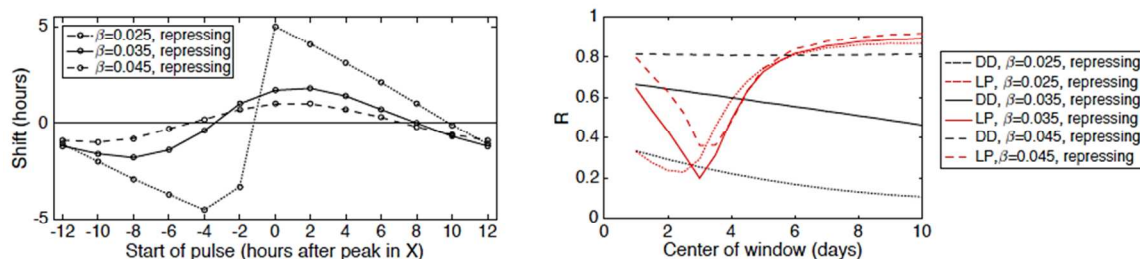
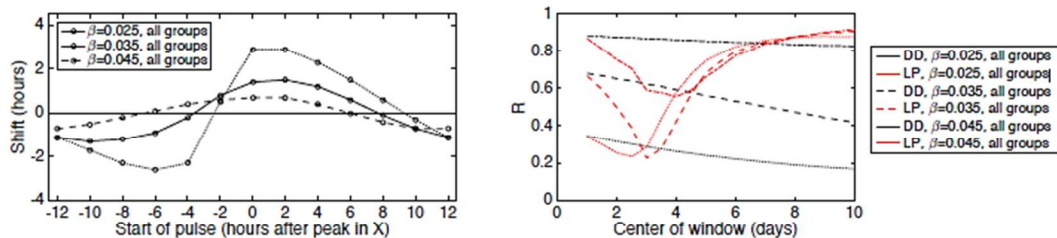**Figure M11. Coupling from all three groups is repressing.**

Figure M12. All groups (10 in group 1, 10 in group 2, 40 in group 3).
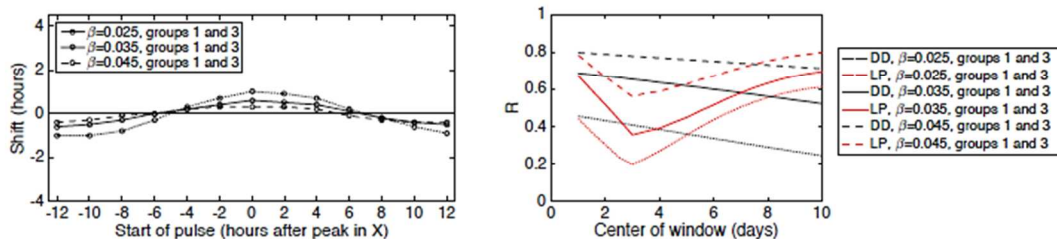

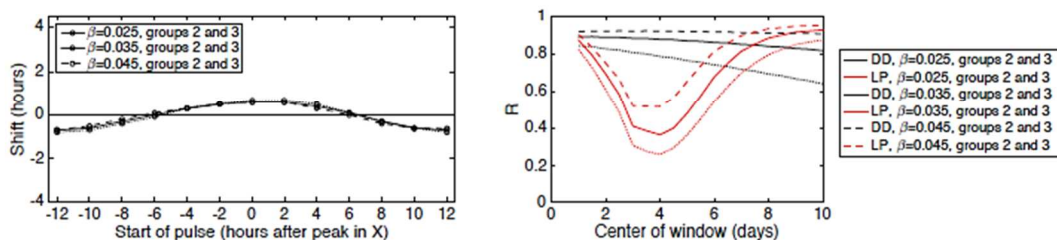Figure M13. Groups 1 and 3 only (20 in group 1, 40 in group 3).

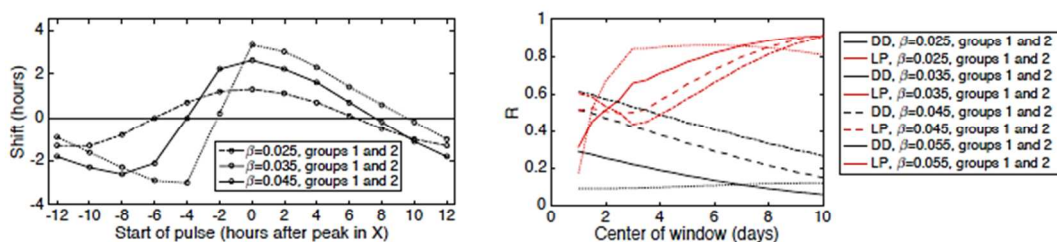Figure M14. Groups 2 and 3 only (20 in group 2, 40 in group 3).

Figure M15. Groups 1 and 2 only (30 in group 1, 30 in group 2).

Left: Phase response curve for a 30-minute light pulse. Negative shifts indicate delays, while positive shifts correspond to advances.

Right: Order parameter R, calculated using Z, in DD versus following a 4h light pulse that begins 3 hours before peak in X, which results in a large phase advance.
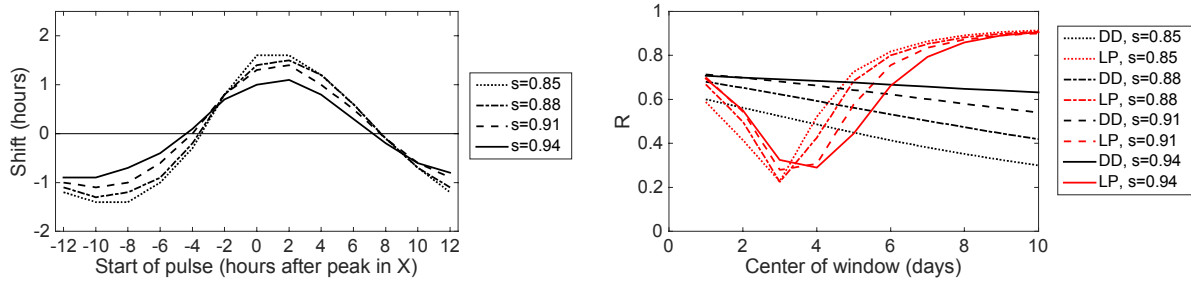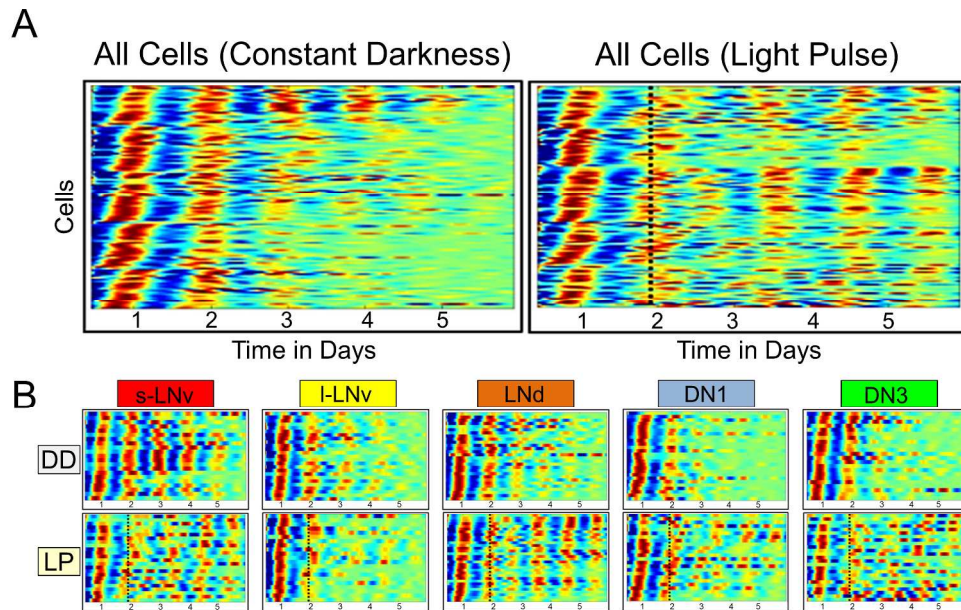
Figure M16. Effect of group 3's mean damping rate in mixed coupling system with all groups. Increasing the mean value of *s* in group 3 results in a system that is more resistant to shifting and that exhibits a higher order parameter. (Lower *s* results in faster damping.)
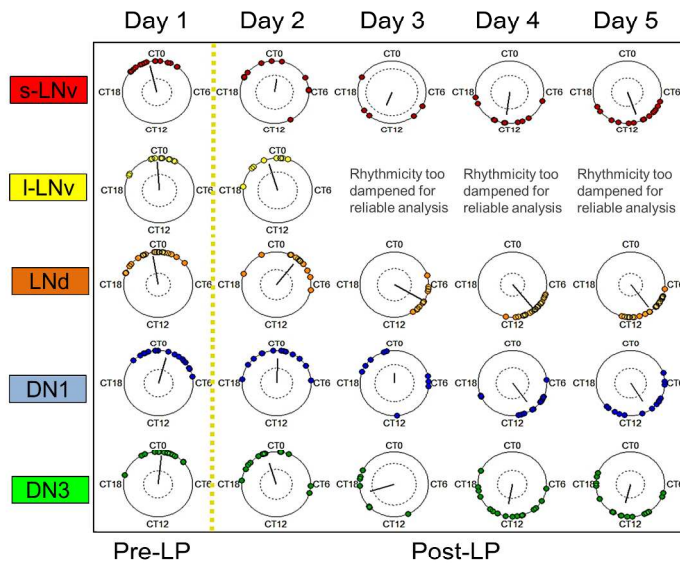
References

Bliss RD, Painter PR, and Marr AG (1982) Role of feedback inhibition in stabilizing the classical operon. Journal of Theoretical Biology 97:177-193.

Cheng Z, Liu F, Zhang XP, Wang W (2009) Reversible phosphorylation subserves robust circadian rhythms by creating a switch in inactivating the positive element. Biophys J 97: 2867–2875.

Collins B, Kaplan HS, Cavey M, Lelito KR, Bahle AH, Zhu Z, Macara AM, Roman G, Shafer OT, and Blau J (2014) Differentially timed extracellular signals synchronize pacemaker neuron clocks. PLoS Biol 12(9): e1001959.

Dissel S, Hansen CN, Özkaya Ö, Hemsley M, Kyriacou CP, and Rosato E (2014) The logic of circadian organization in *Drosophila*. Current Biology 24:2257-2266.

Gonze D, Bernard S, Waltermann C, Kramer A, and Herzel H (2005) Spontaneous synchronization of coupled circadian oscillators. Biophys J 89:120-129.

Gu C, Ramkisoensing A, Liu Z, Meijer J, and Rohling J (2014) The proportion of light-responsive neurons determines the limit cycle properties of the Suprachiasmatic Nucleus. J Biol Rhythms 29(1):16-27.

Gu C, Xu J, Rohling J, Yang H, and Liu Z (2015) Noise induces oscillation and synchronization of the circadian neurons. PLoS ONE 10(12): e0145360.

Kidd PB, Young MW, and Siggia ED (2015) Temperature compensation and temperature sensation in the circadian clock. Proceedings of the National Academy of Sciences 112(46):E6284-E6292.

Komin, N (2011) Synchronization and entrainment of coupled circadian oscillators. Interface Focus 1(1):167-176.

Leise TL, Wang CW, Gitis PJ, Welsh DK (2012) Persistent Cell-Autonomous Circadian Oscillations in Fibroblasts Revealed by Six-Week Single-Cell Imaging of PER2::LUC Bioluminescence. PLoS ONE 7(3): e33334.

Ruoff P, Vinsjevik M, Monnerjahn C, and Rensing L (2001) The Goodwin model: simulating the effect of light pulses on the circadian sporulation rhythm of *Neurospora crassa*. J Theoretical Biology 209(1): 29-42.

Saithong T, Painter K, Millar AJ (2010) The contributions of interlocking loops and extensive nonlinearity to the properties of circadian clock models. PLoS One 5: e13867.

Tokuda, I. T., Ono, D., Ananthasubramaniam, B., Honma, S., Honma, K. I., & Herzel, H. (2015). Coupling Controls the Synchrony of Clock Cells in Development and Knockouts. Biophysical journal, 109(10), 2159-2170.

Tyson JJ (2002) Biochemical oscillations. In Computational Cell Biology, pp 230-260, Springer.

Yao Z, and Shafer O (2014) The *Drosophila* circadian clock is a variably coupled network of multiple peptidergic units. Science 343:1516-1520.

15

A

All Cells (Constant Darkness)   **All Cells (Light Pulse)**
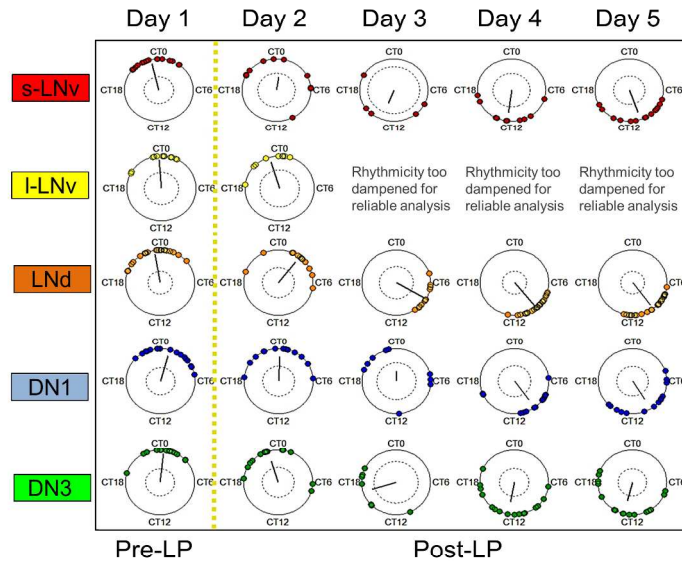

B   s-LNv   l-LNv   LNd   DN1   DN3

Circadian neurons of cultured whole brain explants exhibit distinct dynamic signatures in constant darkness and when exposed to a phase advancing light pulse. Pseudo-heat maps of individual oscillator XLG-Per-Luc expression over time are provided for A: 'all cells' (combined across 12 brains per condition) and B: each neuronal subgroup. Warmer colors indicate higher amplitude whereas cooler colors indicate lower amplitude of rhythmic Per expression. A (Left): Cells in DD (n=122) exhibit a wide range of free-running phases with decreasing phase coherence over time. A (Right): Cells (n=126) exposed to a 15 min 12.57 W/m2 white light pulse (LP) at CT 22 on the second day in DD (indicated by dotted black line) generally exhibit a transient reduction in phase coherence and amplitude followed by a phase shift and gradual recovery of phase coherence and amplitude over time. B (Top): L-LNvs (n=25), LNds (n=28), DN1s (n=26), and DN3s (n=22) in DD generally exhibit a loss of phase coherence and amplitude over time to varying degrees with the s-LNvs (n=21) exhibiting the most consistent and robust phase coherence. B (Bottom): S-LNvs (n=24), l-LNvs (n=25), DN1s (n=26), and DN3s (n=22) exposed to the LP exhibit distinct dynamic signatures of transient loss followed by delayed recovery of phase-shifted oscillator synchrony (phase retuning) and amplitude following the LP. Note that the LNds (n=28) appear to exhibit relatively consistent phase coherence and amplitude following the LP, as well as the most rapid phase shift. Raster plots were generated using custom MATLAB scripts analyzing bioluminescence data reported previously (Roberts et al., 2015).
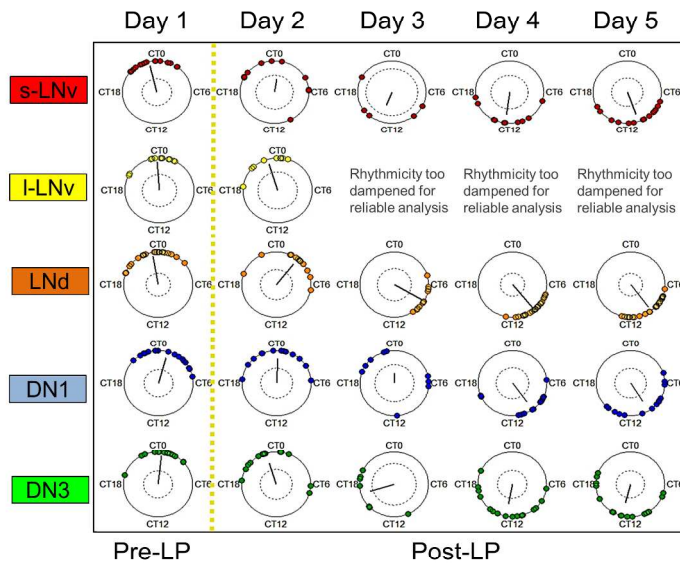
254x190mm (300 x 300 DPI)

Neuronal subgroups exposed to a phase-advancing light pulse exhibit distinct dynamics of loss and recovery of phase-shifted synchronous oscillations. Circular phase plots reveal distinct neuronal subgroups' dynamics of phase response to a light pulse (the yellow dotted line divides the general time frames of pre-LP and post-LP exposure). Neuronal subgroups generally exhibit significant phase dispersion following exposure to the LP, with the exception of the LNds and DN3s. Relative to corresponding subgroups in DD, neuronal subgroups also generally exhibit significantly greater phase coherence and a shift in mean phase 3-4 days after the light pulse. The inner circles represent the the $\alpha = 0.05$ threshold for each Rayleigh test, with the null hypothesis that phases are uniformly distributed.
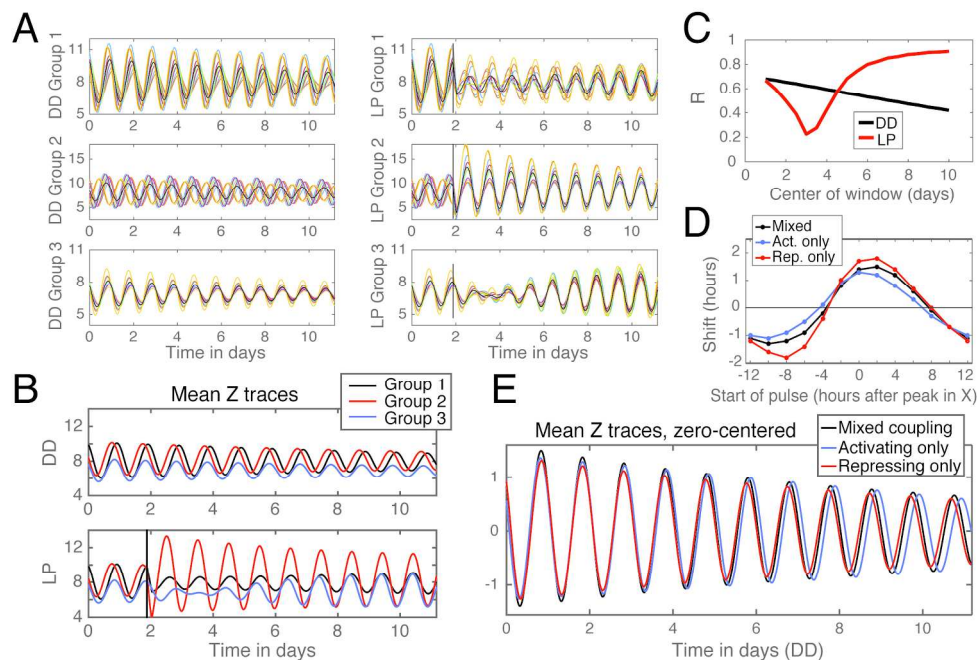254x190mm (300 x 300 DPI)

Neuronal subgroups exposed to a phase-advancing light pulse exhibit distinct dynamics of loss and recovery of phase-shifted synchronous oscillations. Circular phase plots reveal distinct neuronal subgroups' dynamics of phase response to a light pulse (the yellow dotted line divides the general time frames of pre-LP and post-LP exposure). Neuronal subgroups generally exhibit significant phase dispersion following exposure to the LP, with the exception of the LNds and DN3s. Relative to corresponding subgroups in DD, neuronal subgroups also generally exhibit significantly greater phase coherence and a shift in mean phase 3-4 days after the light pulse. The inner circles represent the the α =0.05 threshold for each Rayleigh test, with the null hypothesis that phases are uniformly distributed.
254x190mm (300 x 300 DPI)

Neuronal subgroups exposed to a phase-advancing light pulse exhibit distinct dynamics of loss and recovery of phase-shifted synchronous oscillations. Circular phase plots reveal distinct neuronal subgroups' dynamics of phase response to a light pulse (the yellow dotted line divides the general time frames of pre-LP and post-LP exposure). Neuronal subgroups generally exhibit significant phase dispersion following exposure to the LP, with the exception of the LNds and DN3s. Relative to corresponding subgroups in DD, neuronal subgroups also generally exhibit significantly greater phase coherence and a shift in mean phase 3-4 days after the light pulse. The inner circles represent the the α =0.05 threshold for each Rayleigh test, with the null hypothesis that phases are uniformly distributed.

254x190mm (300 x 300 DPI)

Mathematical modeling of circadian network dynamics indicates importance of complementary coupling of strong and weak oscillators in synchronization and adaptation. The general dynamic signatures of oscillator synchrony and phase retuning by light are modeled using three oscillator groups coupled by complementary activating and repressing signals. A: Three oscillator groups (60 oscillators total) are simulated in either constant darkness (A, Left) or in response to a phase advancing light pulse (A, right), using a modified version of the Goodwin model (Tyson, 2002). Traces of the Z variable are shown here. Rate parameters are set to generate damped circadian oscillations. Group 1 (10 oscillators) is light responsive and sends a signal that increases transcription rate. Group 2 (10 oscillators) is light responsive, has a shorter period, and sends a signal that decreases transcription rate. Group 3 (40 oscillators, but only 10 representative oscillators shown in figures for clarity) is not directly light responsive, more strongly damped, and send a signal that decreases transcription rate. B: Mean traces of the Z variable from each of the three groups of oscillators show that group 2 oscillators exhibit an increase in amplitude following the LP and are the first group to exhibit a phase advance. C: As observed with bioluminescence data, the simulated oscillators exposed to a phase advancing light pulse (red trace) exhibit a mean decrease in order parameter R, followed by a delayed increase in R relative to oscillators in DD (black trace). R varies between 0 and 1 with higher values indicating similarity in phase, period, and waveform. D: Phase response curves of simulated systems, with all oscillators having only excitatory signals (activating only), only inhibitor signals (repressing only), or a complementary system with a mix of both signaling types. E: Simulations in constant darkness show that the complementary system shows an intermediate period length relative to activating only and repressing only systems. Simulations were generated using custom MATLAB scripts. See Materials and Methods for details.

205x137mm (300 x 300 DPI)